Process simulation and energy analysis of synthetic natural gas production from water electrolysis and CO2 capture in a waste incinerator

Applied Energy 343 (2023) 121200

Contents lists available at ScienceDirect

Applied Energy

journal homepage: www.elsevier.com/locate/apenergy

# Process simulation and energy analysis of synthetic natural gas production from water electrolysis and $CO_2$ capture in a waste incinerator

Fabio Salomone [a,*,1], Paolo Marocco [b,1], Daniele Ferrario [b,1], Andrea Lanzini [b], Debora Fino [a], Samir Bensaid [a], Massimo Santarelli [b]

[a] Department of Applied Science and Technology (DISAT), Polytechnic of Turin, Corso Duca degli Abruzzi 24, 10129 Turin, Italy
[b] Department of Energy (DENERG), Polytechnic of Turin, Corso Duca degli Abruzzi 24, 10129 Turin, Italy

## HIGHLIGHTS

- Analysis of the reuse of $CO_2$ from a waste incinerator in a power-to-gas system.
- Different carbon capture and electrolysis technologies are considered.
- Detailed modelling of all sections of the power-to-gas system is performed.
- KPIs are presented to investigate the energy and environmental performance.
- A comparative assessment of the different power-to-gas configurations is provided.

## GRAPHICAL ABSTRACT

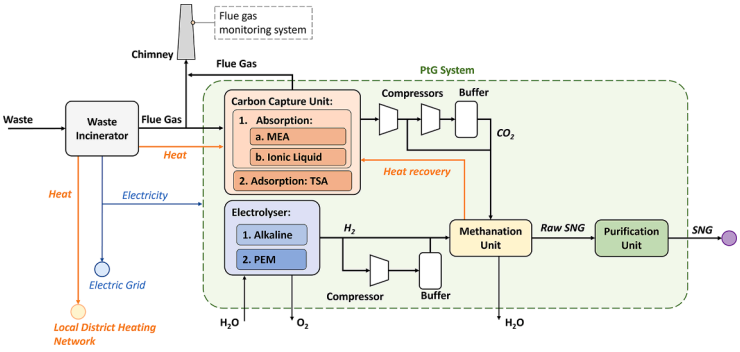


## ARTICLE INFO

*Keywords:*
Power-to-gas
Carbon capture and utilization
Electrolysis
Methanation
Thermal integration
Hydrogen

## ABSTRACT

Power-to-gas (PtG) and carbon capture and utilisation are expected to play a key role in promoting a sustainable energy transition. In this work, a detailed energy analysis of a complete PtG system integrated with a real waste incinerator is performed. A fraction of the renewable electricity and heat produced by the waste incinerator is used in the PtG system to produce hydrogen, which is further converted into SNG by methanation with $CO_2$ recovered from the plant flue gases. A PtG plant able to produce up to 500 $m^3$/h of SNG is considered. A total of six different plant configurations are analysed, obtained by the combination of different electrolysis and post-combustion carbon capture technologies. Specifically, alkaline and PEM electrolysers are considered for the production of hydrogen, while absorption with monoethanolamine solution, absorption with monoethanolamine and ionic liquid solution, and temperature swing adsorption with solid sorbent are selected for carbon capture. The main sections of the PtG system are modelled and the performance of the overall system is evaluated by computing key performance indicators, such as the global energy efficiency and the Specific Plant Energy Consumption for $CO_2$ Avoided (SPECCA). Special attention is also paid to the thermal integration between the methanation unit and the carbon capture unit. The heat produced during the methanation process is sufficient to cover the entire heat demand of the $CO_2$ capture unit in almost all configurations investigated. In particular, thermal integration increases the global energy efficiency by 5–9% and reduces the SPECCA indicator by 5–8%.

* Corresponding author.
*E-mail address:* fabio.salomone@polito.it (F. Salomone).
[1] These authors contributed equally to this work.

https://doi.org/10.1016/j.apenergy.2023.121200
Received 21 December 2022; Received in revised form 31 March 2023; Accepted 21 April 2023
Available online 11 May 2023

Considering the thermally integrated configurations, the global energy efficiency is estimated to be between 44.6% and 46.7%, while the SPECCA value ranges from 40.5 MJ/kg to 42.4 MJ/kg. Finally, some technical considerations are given, including the quality of SNG produced and the degradation phenomena in the considered technologies.

**Nomenclature**

*Acronyms and Abbreviations*

| | |
|---|---|
| ALK | Alkaline |
| BoP | Balance of Plant |
| [bpy][$BF_4$] | 1-Butylpyridinium tetrafluoroborate |
| CC | Carbon Capture |
| CCU | Carbon Capture and Utilization |
| Conf. | System configuration |
| Const. | Constant |
| Eff. | Efficiency |
| EL | Electrolyser |
| GHG | Greenhouse Gas |
| IL | Ionic Liquid |
| LHHW | Langmuir-Hinshelwood-Hougen-Watson |
| LHV | Lower Heating Value |
| MEA | Monoethanolamine |
| NTP | Normal Temperature and Pressure |
| PCC | Post-combustion Carbon Capture |
| PEI | Polyethylenimine |
| PEM | Polymer Electrolyte Membrane |
| PMMA | Polymethylmethacrylate |
| PtG | Power-to-Gas |
| PtX | Power-to-X |
| RCC | Ratio of $CO_2$ Captured |
| RES | Renewable Energy Sources |
| SNG | Synthetic Natural Gas |
| SPECCA | Specific Plant Energy Consumption for $CO_2$ Avoided |
| STP | Standard Temperature and Pressure |
| TSA | Temperature Swing Adsorption |
| WI | Waste Incinerator |

## 1. Introduction

Carbon dioxide is one of the major greenhouse gases (GHG) responsible for global warming. $CO_2$ released from combustion and manufacturing processes contributed to about 78% of the increase in GHG emissions between 1970 and 2010 [1]. Immediate action at the global level through coordinated and cooperative responses is needed to significantly reduce GHG emissions and mitigate the risks related to climate change. Under the framework of the Paris Agreement, in force since 2020, governments have committed to keeping global temperatures well below 2 °C above the pre-industrial average level. European Union has launched the Green Deal as a response to the challenge of UN 2030 Agenda for Sustainable Development for a green transition. The Green Deal is based on several pillars, of which "clean energy" and "sustainable industry" are the main actions required by the manufacturing and production sectors of economy. The ultimate objective of this strategy is the carbon neutrality by 2050, where a key role will be played by the use of renewable energy sources (RES) and the decarbonisation and modernization of energy-intensive industries through carbon capture, utilization and storage technologies.

Renewable energy sources will most likely make up the majority of the future energy mix to reduce GHG emissions and counteract the ongoing depletion of fossil fuels. However, well-known issues, related to electric grid management and energy storage, must be resolved for RES to be deployed on a large scale. Power-to-gas (PtG) is expected to be necessary in future renewable energy systems [2], as it provides the flexibility needed with increasing production of intermittent renewable power [3]. Sector coupling through PtG is fundamental for the transformation of the European energy system, contributing to the transition to a low-carbon economy [4,5]. As a general definition, PtG refers to the storage of the excess renewable energy in the form of chemical potential of gaseous substances. In particular, the conversion of RES to hydrogen and then to synthetic natural gas (SNG) is one of the most common PtG pathways, which allows the storage and transport of renewable energy via the exiting gas infrastructure [6].

Hydrogen, which can be produced by water electrolysis using renewable energy, represents a promising storage solution (besides being a green feedstock for industry) due to its long-term storage capability and high energy density [7]. Alkaline (ALK) electrolysis is currently the most cost-effective electrolysis technology; however, in the near future, polymer electrolyte membrane (PEM)-based solutions may be more suitable for the PtG route [8]. To complete the PtG pathway [8–10], hydrogen should be further converted to synthetic natural gas by reacting with an on-site carbon feedstock. For instance, $CO_2$ from fossil-fired plants could be used in linear carbon capture and utilization (CCU) systems, while circular CCU schemes exploit $CO_2$ from renewable sources (e.g., biofuel combustion, direct air capture), resulting in reduced GHG emissions and fossil fuel consumption [11].

Carbon capture can be achieved by absorption, adsorption and membrane separation processes [12,13]. Absorption technologies employ water, ethanolamine, ammonia or ionic liquids as absorbents [14]. Currently, there are several industrial processes based on $CO_2$ absorption, such as the Kerr-McGee/AGG Lummus Crest (KMALC) process, the Fluor's Econamine FG Plus$^{SM}$ (Fluor EFG +) process, the Kansai Mitsubishi Carbon Dioxide Recovery (KM CDR) process, aqueous or chilled ammonia processes, and dual or strong alkali absorption processes [14]. Concerning monoethanolamine (MEA) and ionic liquid (IL) aqueous solutions, the specific thermal energy consumption required for regeneration ranges from 3.7 MJ/$kg_{(CO2)}$ to 4.8 MJ/$kg_{(CO2)}$, and high $CO_2$ purities, recoveries and productivities can be attained [15]. Adsorption technologies, on the other hand, are at demonstration scale and exploit the affinity of solid sorbents (e.g., zeolites, active carbon or functionalised porous materials) with the $CO_2$. Temperature swing adsorption, pressure swing adsorption, vacuum swing adsorption or combined processes can achieve high $CO_2$ purities and recoveries by reducing the specific thermal energy requirements from 3.3 MJ/$kg_{(CO2)}$ to 4.3 MJ/$kg_{(CO2)}$ [16]. Finally, the membrane separation processes are in a demonstration stage of development, and the major disadvantage is the high electrical power consumption for compressing the gases, which can be as high as 1.2 MJ/$kg_{(CO2)}$ [17].

SNG is obtained from hydrogen and carbon dioxide through the methanation process, which is based on the Sabatier reaction [8,18–25]. This process has been widely studied in the literature and the most active, selective and stable catalyst is Ni/γ-$Al_2O_3$, which is commercially available [18,26–28]. Methanation is strongly exothermic and occurs at medium–high temperatures (250 °C to 600 °C). Thermal management is therefore a crucial aspect of the methanation section [20,23,24].

In this work, a comprehensive model of a complete PtG system downstream of a real waste incinerator (WI) is presented. This kind of integration allows for: (i) reuse of the waste $CO_2$ produced during the combustion processes; (ii) decentralised production of green SNG using biogenic $CO_2$ and renewable electricity generated in the WI; (iii) an easier coupling with a PtG system due to lower fluctuations in electricity production; (iv) production of valuable product (SNG) that can be sold in different markets (natural gas grid, transport sector, etc.).

In this analysis, the possibility of thermal integration through the PtG plant sections is also evaluated (i.e., between carbon capture and methanation units) to improve the plant efficiency and reduce the dependence on external heat sources. Detailed modelling of all the PtG sections was performed to accurately estimate the performance of the overall system. Three different technologies for $CO_2$ capture, i.e., absorption with both MEA and IL-MEA aqueous solutions and adsorption on solid sorbents, were investigated. In addition, both PEM and alkaline electrolysers were considered for hydrogen production. The technical feasibility of the system was demonstrated with a one-year energy simulation using the real operating data of a waste incinerator (net power production, operating hours, flue gas flow rate and composition). Different technologies and layout options were comparatively analysed to provide a complete picture of the technical viability of the main PtG system configurations.

Although PtG systems and $CO_2$ methanation have been extensively studied in the past, there is still a lack of studies that perform a thorough process modelling of the overall PtG plant and compare different technological solutions. Table 1 shows the most recent works available in the literature in which a process analysis is carried out at the plant level. Most authors have not included the carbon capture unit in their model; furthermore, one or more sections of the PtG plant are often modelled with a simple black-box approach where fixed efficiency values are considered. Giglio *et al.* [20,23,29], Salomone *et al.* [24] and more recently Haider *et al.* [30] studied the integration between hydrogen production from SOEC and methanation with adiabatic and cooled reactors; however, they did not include the carbon capture section in their study. Gorre *et al.* [5,31], similarly, performed some techno-economic analyses, considering only the electrolyser and the methanation units and assuming fixed values for the efficiencies of both sections. Morosanu *et al.* [25] and Chauvy *et al.* [32,33], analysed the system performance considering all the plant sections; but, not all were modelled in detail. To the best of our knowledge, the present work represents thus the most comprehensive and thorough process study currently available on the topic. Furthermore, no previous work has been found that addresses the integration of a PtG system into a real waste incinerator plant.

## 2. Description and modelling of the PtG sections

Fig. 1 shows a block diagram of the PtG system that includes three main sections: (i) the carbon capture unit, (ii) the electrolyser and (iii) the methanation unit.

The $CO_2$ produced in the WI is first removed from the flue gas in a post-combustion carbon capture (PCC) unit. Two different post-combustion carbon capture technologies were considered: an absorption system based on liquid sorbents, and an adsorption system based on solid sorbents. The captured $CO_2$ is then converted into synthetic methane by reaction with hydrogen in the methanation unit, which consists of refrigerated tube-bundle fixed bed catalytic reactors. The hydrogen needed for the methanation reaction is obtained from water through alkaline or PEM electrolysis. The electricity consumed by the PtG process is supplied directly by the waste incinerator power plant. Hydrogen and $CO_2$ buffers allow continuous operation in case of maintenance/failures or electricity supply shortage from the WI. The synthetic natural gas is finally treated in the purification unit to remove unconverted hydrogen and water moisture, thus achieving natural gas grid specifications [34].

The PtG system performance was estimated by considering an SNG productivity of 500 $m^3_{(NTP)}/h$ as nominal size, which is within the range of availability of electrical energy generated by the combustion of the biomass fraction of the waste. This sizing therefore avoids possible indirect $CO_2$ emissions due to the consumption of non-renewable electrical energy. Fig. 2 summarises all PtG configurations (Conf.) considered in this work.

### 2.1. Waste incinerator system

The WI considered here is located in Italy and produces electricity and heat. The high-pressure steam (60 bar and 420 °C) obtained from the flue gas cooling is fed to a steam turbine. Steam at 16 bar and 120 °C is spilled from the turbine and is used in the local district heating network. The cooled flue gases pass through several stages of emission abatement before being released to the atmosphere: electrostatic precipitation of particulate, neutralisation of acid gases, dioxins, furans and heavy metals, dust removal by bag filters and selective catalytic reduction of $NO_x$. The cleaned flue gases are then continuously analysed

**Table 1**
Model details of previous plant level assessment works regarding SNG production from captured $CO_2$ and electrolysis.

| Reference | | $CO_2$ source | Carbon Capture Technology (Model) | Electrolyser Technology (Model) | Methanation Technology (Model) |
|---|---|---|---|---|---|
| Giglio *et al.* 2015a | [23] | Not specified | – | SOEC (electrochemical) | Adiabatic reactors (equilibrium) |
| Giglio *et al.* 2015b | [29] | Not specified | – | SOEC (electrochemical) | Adiabatic reactors (equilibrium) |
| Giglio *et al.* 2018 | [20] | Not specified | – | SOEC (electrochemical) | Cooled reactors (kinetic) |
| Morosanu *et al.* 2018 | [25] | Air | Adsorption (const. eff.) | ALK (const. eff.) | Adiabatic and Cooled reactors (experimental eff.) |
| Gorre *et al.* 2019 | [31] | Not specified | – | Not specified (const. eff.) | Not specified (const. eff.) |
| Salomone *et al.* 2019 | [24] | Not specified | – | SOEC (const. eff.) | Cooled reactors (const. eff.) |
| Chauvy *et al.* 2020 | [32] | Cement | Absorption (kinetic) | PEM (const. eff.) | Adiabatic reactors (kinetic) |
| Gorre *et al.* 2020 | [5] | Not specified | – | ALK (const. eff.) | Cooled reactors (const. eff.) |
| Chauvy *et al.* 2021 | [33] | Cement | Absorption (kinetic) | PEM (const. eff.) | Adiabatic reactors (kinetic) |
| Haider *et al.* 2022 | [30] | Not specified | – | SOEC (const. eff.) | Adiabatic reactors (kinetic) |
| Present work | | Waste Incinerator | Absorption and Adsorption (kinetic) | ALK and PEM (electrochemical) | Cooled reactors (kinetic) |

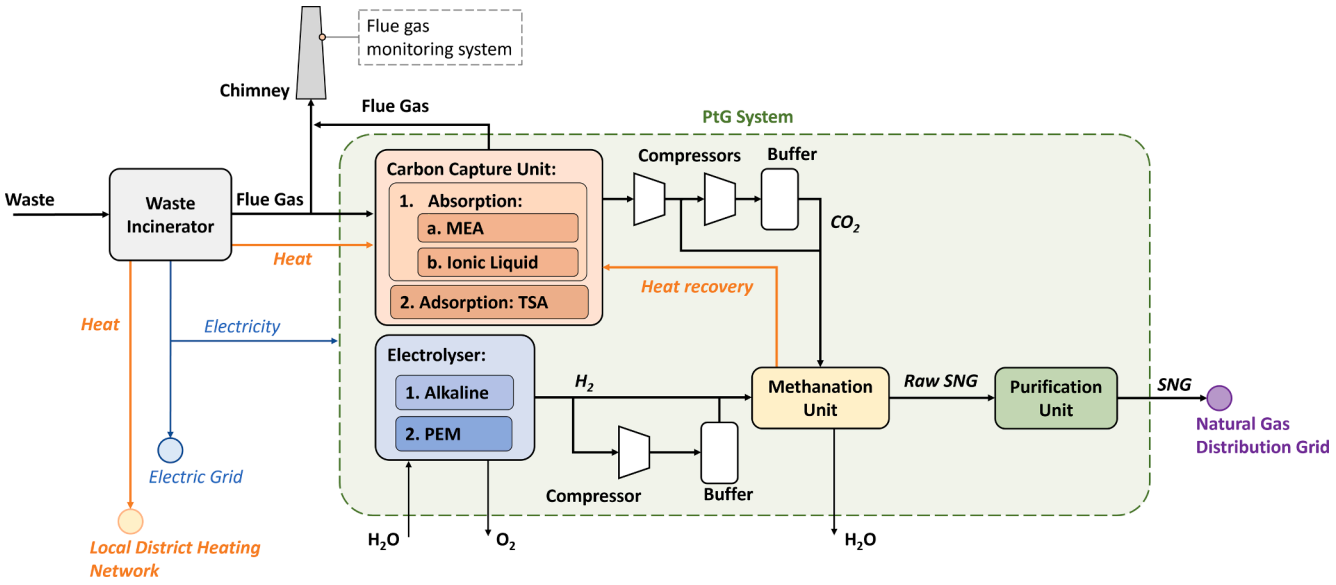


**Fig. 1.** Layout of the power-to-gas system.

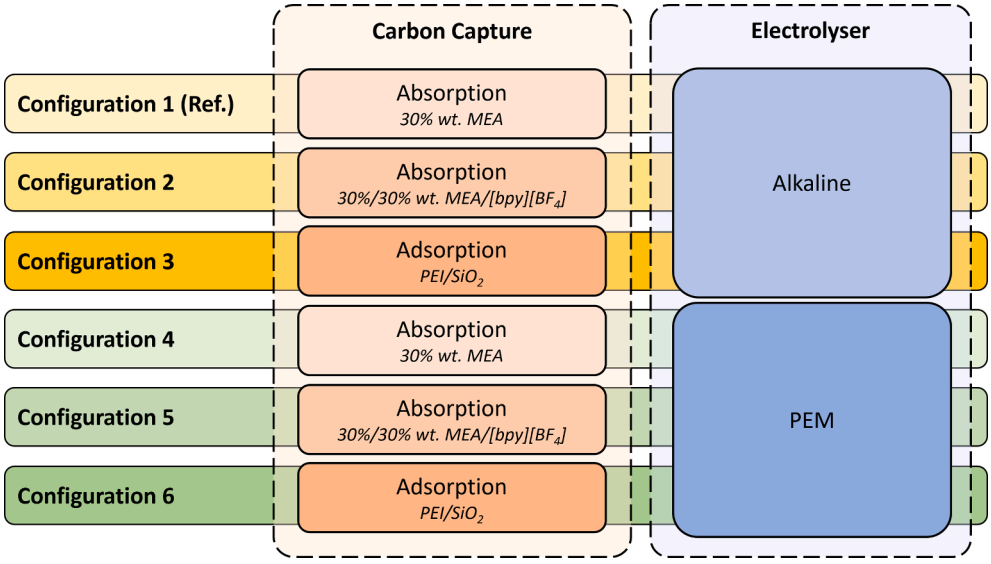


**Fig. 2.** Overview of PtG system configurations analysed in this work.

before their release at the chimney to guarantee compliance with emission limits. The average macro-composition of the flue gases is reported in Table 2. A typical annual composition dataset was considered in the mass and energy balance calculations of this analysis. The presence of pollutants and contaminants (i.e., CO, $NH_3$, $NO_x$, $SO_x$, etc.) was neglected. The annual plant operating time was assumed to be 7879 h/y, to account for programmed or temporary stops for maintenance.

### 2.2. Carbon capture system

Different technologies are available for the capture of $CO_2$ from exhaust gases, such as absorption, adsorption, and membrane separation systems. In this work, as shown in Fig. 2, we considered the integration of three different carbon capture techniques:

**Case 1.**

**Table 2**
Average operating data and flue gas characteristics of the waste incinerator.

| Parameter | Value | Unit | Parameter | Value | Unit |
|---|---|---|---|---|---|
| Operative time | 7879 | h/y | Flue gas composition | | |
| $CO_2$ emissions | 190 ± 73 | kt/y | $CO_2$ | 9.7 ± 3.1 | vol.% |
| Flue gas temperature | 118 ± 26 | °C | $O_2$ | 10.1 ± 3.3 | vol.% |
| Flue gas pressure | 0.978 ± 0.001 | bar | $H_2O$ | 17.1 ± 4.9 | vol.% |
| Biomass-derived (renewable) energy (electricity and heat) | 51.0 | % | $N_2$ | 63.1 ± 6.6 | vol.% |

**a.** Absorption process using a liquid solvent based on an aqueous solution with 30 wt% monoethanolamine (MEA), here called solvent A. This technology has been extensively studied in the past and can be considered the reference system for PCC [35].

**b.** Absorption process using a liquid solvent based on an aqueous solution with 30 wt% MEA and 30 wt% IL, consisting of 1-Butylpyridinium tetrafluoroborate ([bpy][$BF_4$]), to increase the system performances, solvent B [36].

**Case 2.**

Temperature swing adsorption (TSA) process using a solid adsorbent based on functionalised porous support (i.e., PEI/$SiO_2$).

The extracted $CO_2$ is then compressed to 15 bar and sent to the methanation unit. Furthermore, a $CO_2$ storage tank (in liquid form, 80 bar) guarantees the proper operation of the SNG production system in case of any short interruptions of the WI. The isentropic and electro-mechanical efficiencies of the $CO_2$ compressors were set at 0.75 and 0.95, respectively [23].

### 2.2.1. Absorption carbon capture unit

Absorption systems are the most mature PPC technologies and the only ones that have reached the stage of commercialisation. They are based on liquid solvents circulating between an absorption and a desorption column. In this regard, aqueous MEA solutions are the most commonly employed solvents, characterised by low costs but relatively high regeneration energy and low $CO_2$ absorption capacity. For these reasons, other more performing solvents have also been proposed in the literature. Among these, ionic liquids are those with the most promising properties for $CO_2$ absorption, such as: (i) very low volatility; (ii) high thermal stability; (iii) high $CO_2$ absorption capacity and (iv) low heat capacity. Due to these characteristics, the use of an absorption carbon capture system employing an IL-based solvent can reduce the system regeneration heat duty and the solvent losses in the treated flue gas [36–38].

As schematised in Fig. 3, $CO_2$ removal occurs in a packed absorption column where the flue gases flow upward, in counter-current with the solvent coming from the top. The $CO_2$-poor gas leaves the upper part of the absorber, while the $CO_2$-rich solvent leaves the column from the bottom. The solvent is then pumped and heated up and sent to the stripper, where nearly pure $CO_2$ (99.6% w/w) is separated from the liquid and exits the column head. The regenerated sorbent is cooled and recirculated back to the absorber after being mixed with fresh solvent and water to balance the leakage for entrainment and evaporation in the stripper and absorber.

The flue gases are extracted upstream of the incinerator chimney at 117.6 °C and 0.978 bar and directly sent to the absorber column. Usually, the flue gases are first sent to a cooling section as low temperatures are recommended to improve $CO_2$ absorption. Using flue gases at a high temperature, however, limits the corrosion phenomena in the absorber and the needs to install an additional component. This solution, therefore, aims to reduce plant costs and the invasiveness of retrofit measures.

The described process of carbon capture was modelled using Aspen Plus process simulator software. The physical and chemical properties of [bpy][$BF_4$] were taken from recently published studies [36,37,39] and used as input to the model. Non-Random-Two-Liquid model for liquid with Redlich-Kwong equation of state for vapour were adopted to evaluate the thermodynamic properties of the mass streams.

The reactions describing the chemical interaction between $CO_2$ and the liquid sorbent are listed in Table 3. It should be noted that [bpy][BF4] does not chemically react with the $CO_2$, therefore the reactions considered are the same for both the absorption systems considered.

The coefficients for the equilibrium constants of reactions R1-R3 (Table 3) were determined according to Eq. (1). Kinetic rates were used instead for the reactions R4-R7 (Table 3); they were estimated through Eq. (2), employing the coefficients proposed by Canepa *et al.* [40]. The coefficients used to estimate the equilibrium constants and kinetic rates are reported in Table 4.

$$ln\left(K_{eq}\right) = A + \frac{B}{T} + C \cdot ln(T) + D \cdot T \tag{1}$$

$$r = kT \cdot exp\left(-\frac{E}{RT}\right) \prod_{i=1}^{N} C_i^{a_i} \tag{2}$$

The absorption and desorption packed columns (packing: Flexipac metal 250Y) were sized in order not to exceed the flooding limit of 80% when ensuring a capture efficiency of 75%, considering the flue gas composition given in Table 2. Typical values for the absorption efficiency range from 75% to 95% [15,41]. Considering the amount of $CO_2$ needed for the upstream methanation process and the fact that deep decarbonisation of the process is not the goal of this work, a $CO_2$ capture

**Table 3**
Reactions considered in the absorption system.

| No. | Chemical reaction equation |
|---|---|
| R1 | $2H_2O \leftrightarrow H_3O^+ + OH^-$ |
| R2 | $HCO_3^- + H_2O \leftrightarrow H_3O^+ + CO_3^{2-}$ |
| R3 | $MEAH^+ + H_2O \leftrightarrow MEA + H_3O^+$ |
| R4 | $CO_2 + OH^- \rightarrow HCO_3^-$ |
| R5 | $HCO_3^- \rightarrow CO_2 + OH^-$ |
| R6 | $MEA + CO_2 + H_2O \rightarrow MEACOO^- + H_3O^+$ |
| R7 | $MEACOO^- + H_3O^+ \rightarrow MEA + CO_2 + H_2O$ |

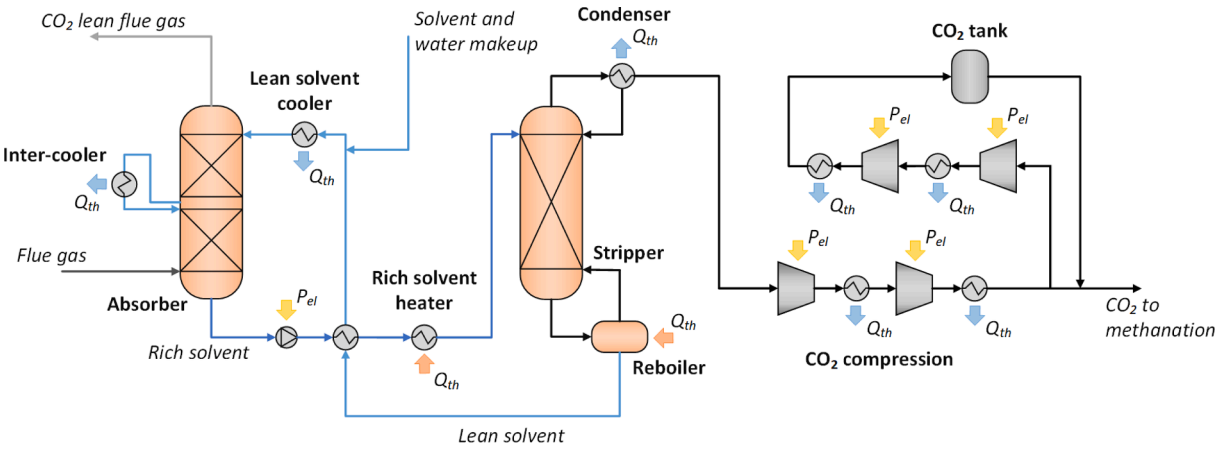


**Fig. 3.** Simplified process scheme of the absorption carbon capture unit.

**Table 4**
Coefficients for equilibrium constants and kinetic rates of reactions R1-R7 [40].

| Reaction | A | B | C | D |
|---|---|---|---|---|
| R1 | 132.889 | −13455.9 | –22.4773 | 0 |
| R2 | 216.049 | −12431.7 | −35.4819 | 0 |
| R3 | −3.03832 | −7008.357 | 0 | $-3.1348 \cdot 10^{-3}$ |
| **Reaction** | **k** | | **E (kJ/mol)** | |
| R4 | $4.32 \cdot 10^{13}$ | | 55.434 | |
| R5 | $2.38 \cdot 10^{17}$ | | 123.223 | |
| R6 | $9.77 \cdot 10^{10}$ | | 41.237 | |
| R7 | $2.18 \cdot 10^{18}$ | | 59.157 | |

efficiency of 75% was chosen for this unit. A height-to-diameter ratio of 10 for the absorption column and 8 for the desorption column was assumed [15,42–44]. Furthermore, an intercooled adsorption column was considered to reduce the solvent flow rate and regulate the liquid temperature [45].

The main operating parameters assumed in the modelling of the carbon capture system section are summarised in Table 5. The $CO_2$ loading of the lean solvent and the condenser pressure of the stripper were determined by sensitivity analyses to minimise the system heat duty and power consumption (the latter is mainly due to $CO_2$ compression).

### 2.2.2. Adsorption carbon capture unit

The second post-combustion carbon capture technology analysed in this work consists of a TSA process based on solid sorbents, which is a promising technique with potentially lower heat demand for sorbent regeneration [16,46–48]. These systems can employ fixed-bed or fluidised bed adsorption columns [16,47]. The main disadvantages of the adsorption processes are the low adsorption capacity, the slowness of the process and the low purity of the produced $CO_2$ stream [49]. Fixed-bed adsorption columns are simple units and there are no liquids that could form corrosive mixtures. Fluidised beds, on the other hand, are integrated in continuous systems designed to cope with thermal issues and optimise the performance of the process; the particle abrasion and the complexity of the separation unit could be some drawbacks [46].

Besides TSA, other adsorption carbon capture technologies have been proposed in the past, such as: vacuum/pressure swing adsorption (V/PSA) and concentration swing adsorption (CSA). CSA is not a suitable technology because $CO_2$ is diluted when a sweep gas is used, reducing the purity of the produced $CO_2$ stream. V/PSA requires a compressor or a vacuum pump, which increases electricity consumption and leaves the heat generated during methanation unused. Therefore, according to the literature [16,46–48], TSA seems to be the best option among adsorption carbon capture technologies.

The most common solid adsorbents are active carbon, zeolites or functionalised porous supports (e.g., PEI/$SiO_2$, PEI/PMMA, PEI/zeolite) [16,46–48]. Zeolites adsorb both $CO_2$ and $N_2$; therefore, the produced $CO_2$ stream contains an inert gas that is difficult to separate [16]. On the other hand, the functionalised supports are characterised by a higher $CO_2$ adsorption capacity [47] and the adsorbent $CO_2$ capture efficiency could achieve 90%. Furthermore, the specific $CO_2$ productivity of functionalised supports is ~ 70 kg/t (against ~ 30 kg/t for zeolites), and a very high $CO_2$ purity of ~ 100% can be achieved if the water vapor contained in the desorbed mixture is condensed after desorption [47].

As shown in Fig. 4, the adsorption $CO_2$ capture unit modelled in this work consists of the following steps:

1. Flue gases from the waste incinerator are cooled from 117.6 °C to 35 °C to condense the water vapour and regulate the temperature of the adsorption column.
2. Carbon capture takes place in parallelised fixed bed columns by using PEI/$SiO_2$.
3. The solid sorbent is regenerated by TSA, recirculating and preheating the $CO_2$-rich stream. This gas stream can be heated up to 200 °C by using the heat recovered in the methanation unit (saturated steam, temperature above 250 °C).
4. The desorbed $CO_2$-rich gases are refrigerated and compressed to 15 bar (operating pressure of the methanation unit) using a multi-stage inter-refrigerated compressor.

The specific adsorbed quantities ($q_i$, mol/kg) of $CO_2$ and $H_2O$ are described by using Eq. (3) and Eq. (4), respectively [16], where $K_i$ is the adsorption constant calculated according to Eq. (5) and $q_{max,CO_2}$ (mol/kg) is the maximum loading of $CO_2$. Looking at Eq. (5), $B_{0,i}$ is the pre-exponential factor, $\Delta h_i$ (J/mol) is the adsorption enthalpy, R (8.314 J/(mol·K)) is the ideal gas constant and T (K) is the temperature. The parameters to estimate the adsorption of $CO_2$ and $H_2O$ on PEI/$SiO_2$ are listed in Table 6.

$$q_{CO_2} = \frac{K_{CO_2} \cdot p_{CO_2}}{1 + K_{CO_2} \cdot p_{CO_2}} \cdot q_{max,CO_2} \tag{3}$$

$$q_{H_2O} = K_{H_2O} \cdot p_{H_2O} \tag{4}$$

$$K_i = B_{0,i} \cdot \exp\left(\frac{-\Delta h_i}{R \cdot T}\right); \quad i = CO_2, H_2O \tag{5}$$

The minimum flue gas flow rate for saturating a column ($\dot{n}_{in,ad,min}$, mol/s) with $CO_2$ was estimated using Eq. (6), while the minimum flue gas flow rate for cooling the column was estimated using Eq. (7),

**Table 5**
Specifics of the absorption carbon capture unit for an SNG production of 500 $m^3_{(NTP)}$/h.

| Parameter | Solvent A | Solvent B | Unit |
|---|---|---|---|
| Inlet flue gas flow rate | $7.8\ 10^3$ | $7.8\ 10^3$ | $m^3_{(NTP)}$/h |
| Liquid solvent composition | 30% MEA | 30%/30% MEA/[bpy][$BF_4$] | wt.% |
| Absorber $CO_2$ capture efficiency | 75 | 75 | % |
| Absorber height | 15 | 15 | m |
| Absorber height-to-diameter ratio [15] | 10 | 10 | – |
| Stripper height | 5.6 | 4 | m |
| Stripper height-to-diameter ratio [15] | 8 | 8 | – |
| Columns' pressure drop | 1 | 1 | kPa |
| Lean solvent loading | 21 | 14 | % |
| Absorber stages number | 20 | 20 | n° stages |
| Stripper stages number | 22 | 22 | n° stages |
| Stripper top pressure | 2 | 3.5 | bar |
| Stripper reboiler temperature | 122 | 142 | °C |
| Stripper solvent recirculation ratio [15] | 10.7 | 10.7 | % |
| Ratio of sorbent sent to the absorber intercooler [15] | 27.5 | 27.5 | % |
| Recirculation pump efficiency | 51 | 51 | % |
| Minimum temperature difference in the recovery heat exchanger | 15 | 15 | °C |

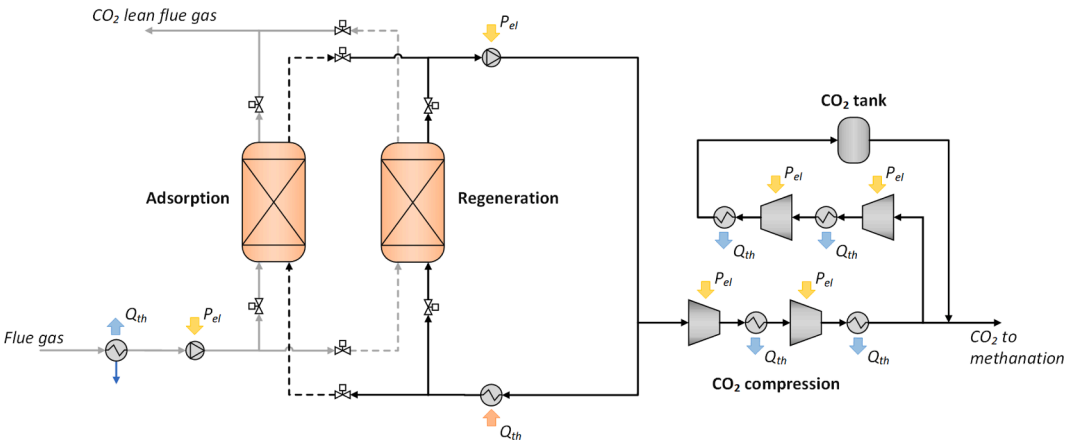


**Fig. 4.** Simplified process scheme of the adsorption carbon capture unit.

**Table 6**
Parameters of the adsorption of $CO_2$ and $H_2O$ on PEI/$SiO_2$ [16].

| Parameter | $CO_2$ | $H_2O$ |
|---|---|---|
| Adsorption enthalpy ($\Delta h_i$) | 91 kJ/mol | 60 kJ/mol |
| Pre-exponential factor ($B_{0,i}$) | $1.25 \cdot 10^{-12}$ 1/bar | $1.61 \cdot 10^{-13}$ mol/(kg·bar) |
| Maximum loading ($q_{max,i}$) | 2.2 mol/kg | – |

obtained from the column mass and energy balance.

$$\dot{n}_{in,ad,min} = \frac{m_s \cdot \left(q_{CO_2,ad} - q_{CO_2,reg}\right)}{y_{CO_2,in} \cdot t_{ad}} \tag{6}$$

$$\dot{n}_{in,th,min} = \frac{m_s \cdot \left[\widehat{c}_{P,s} \cdot \left(T_{reg} - T_{ad}\right) + \sum_i \Delta h_i \cdot \left(q_{i,ad} - q_{i,reg}\right)\right]}{\widetilde{c}_p \cdot \left(T_{reg} - T_{ad}\right) \cdot t_{ad}}; i = CO_2, H_2O \tag{7}$$

where $m_s$ (kg) is the mass of the adsorbent in the column, $q_{i,ad}$ and $q_{i,reg}$ (mol/kg) are the specific adsorbed quantities at adsorption and regeneration conditions, respectively, $y_{CO_2,in}$ is the inlet $CO_2$ molar fraction, $t_{ad}$ (s) is the duration of the adsorption, $\widehat{c}_{P,s}$ (J/(kg·K)) is the specific heat capacity of the adsorbent, $\widetilde{c}_p$ (J/(mol·K)) is the average specific molar heat capacity of the gas, $T_{reg}$ and $T_{ad}$ (K) are the regeneration and adsorption temperatures, respectively. The inlet flow rate was assumed

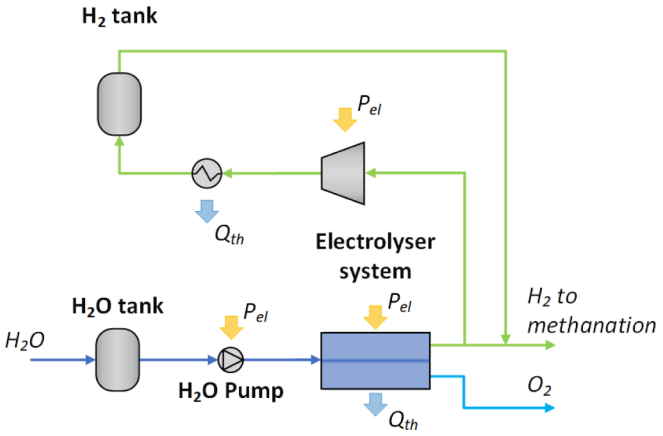


**Fig. 5.** Simplified process scheme of the electrolysis unit.

equal to the higher value between $\dot{n}_{in,ad,min}$ and $\dot{n}_{in,th,min}$ to assure both processes.

Moreover, the minimum gas flow rate for the regeneration, i.e., $\dot{n}_{reg,th,min}$ (mol/s), was computed by performing an energy balance according to Eq. (8), where $t_{reg}$ (s) is the regeneration time.

$$\dot{n}_{reg,th,min} = \frac{m_s \cdot \left[\widehat{c}_{P,s} \cdot \left(T_{reg} - T_{ad}\right) + \sum_i \left(\left(\Delta h_i + \widetilde{c}_{p,i} \cdot \left(T_{reg} - T_{ad}\right)\right) \cdot \left(q_{i,ad} - q_{i,reg}\right)\right)\right]}{\widetilde{c}_p \cdot \left(T_{reg} - T_{ad}\right) \cdot t_{reg}}; \quad i = CO_2, H_2O \tag{8}$$

**Table 7**
Specifics of the adsorption carbon capture unit for an SNG production of 500 $m^3_{(NTP)}$/h.

| Parameter | Value | Unit |
|---|---|---|
| Inlet flue gas flow rate | 10.3 | $km^3_{(NTP)}$/h |
| Adsorber carbon capture efficiency | 56.8 | % |
| Regeneration gas flow rate | 15.32 | t/h |
| Number of columns | 6 | n° columns |
| Adsorption temperature | 40 | °C |
| Regeneration temperature | 200 | °C |
| Adsorption time | 0.5 | h |
| Regeneration time | 0.5 | h |
| Column diameter | 1.65 | m |
| Column height | 1.53 | m |
| Total mass of adsorbent | 6.89 | t |

The scale up of the adsorption columns for achieving the required productivity of $CO_2$ was made considering geometric and fluid-dynamics similarities. Specifically, it was assumed a superficial velocity of 0.42 m/s [47], a useful fraction of the bed length of 71.4% [47] (corresponding to a breakthrough of 90% of the inlet $CO_2$ concentration) and an excess of the inlet flow rate of 10%.

The specifics of the adsorption unit are summarised in Table 7. The adsorption of $CO_2$ was conducted at 40 °C and the regeneration of the adsorption bed was carried out at 200 °C, achieving a $CO_2$ recovery of 97% and a final $CO_2$ purity of 98%. The duration of the adsorption and regeneration processes was assumed to be 0.5 h. The adsorption columns were parallelised (six columns) to reduce their diameter and increase the

flexibility of the system.

### 2.3. Hydrogen production unit

As schematised in Fig. 5, the electrolysis section is composed of the following components:

1. Electrolyser system (stacks + BoP)
2. Water storage tank
3. Pump for water supply
4. Infrastructure for hydrogen compression and storage, i.e., hydrogen compressor, air cooler and hydrogen storage.

Two different low-temperature electrolysis technologies were considered in the analysis: alkaline and PEM. ALK electrolysis represents a mature solution, widely used for large scale industrial applications. ALK systems are also characterised by higher durability (i.e., longer stack life) and lower capital costs compared to the PEM alternative [50]. On the other hand, PEM electrolysis offers higher flexibility, in terms of load range and response time, compared to ALK [51]. PEM electrolysers can also be operated at a much higher current density, which results in greater stack compactness and potentially greater cost reduction. As an example, in Ref. [51] the electrolyser surface area is reported to be about 0.10 $m^2$/kW and 0.05 $m^2$/kW for the alkaline and PEM devices, respectively.

The operating voltage of the electrolysis cell was modelled by the reversible voltage increased by the irreversible losses, including activation, ohmic and diffusion contributions:

$$V_{cell} = V_{rev} + \eta_{act} + \eta_{ohm} + \eta_{conc} \quad (9)$$

where $V_{rev}$ (V) represents the reversible thermodynamic potential, whereas $\eta_{act}$, $\eta_{ohm}$ and $\eta_{conc}$ (V) are the activation, ohmic and concentration overpotentials, respectively. Then, the stack voltage can be computed by summing the voltage of all the series-connected cells that make up the stack.

Experimental polarisation curves from the literature were used to calibrate the electrolyser model and calculate the value of the various fitting parameters. A detailed description of the electrochemical models of both the PEM and ALK systems can be found in the work by Marocco *et al.* [52]. Experimental data from Henao *et al.* [53] were used to validate the alkaline electrolyser model. Data from Han *et al.* [54] were instead considered for the PEM technology.

Faraday's law was employed to determine the amount of hydrogen produced by a single cell, and thus by the stack, under certain operating conditions:

$$\dot{n}_{H_2,cell} = \eta_F \cdot \frac{I}{2 \cdot F} \quad (10)$$

where $\dot{n}_{H_2,cell}$ (mol/s) is the hydrogen molar flow rate produced by the single cell, $\eta_F$ is the Faraday efficiency, $I$ (A) is the operating current and F (C/mol) is the Faraday constant. Regarding the alkaline electrolyser, the Faraday efficiency was computed using a temperature-dependent expression, whose parameters were taken from Ulleberg [55]. The Faraday efficiency of the PEM electrolyser was instead derived by calculating the hydrogen and oxygen fluxes across the PEM membrane [56] and employing the expression given by Tsotridis *et al.* [57].

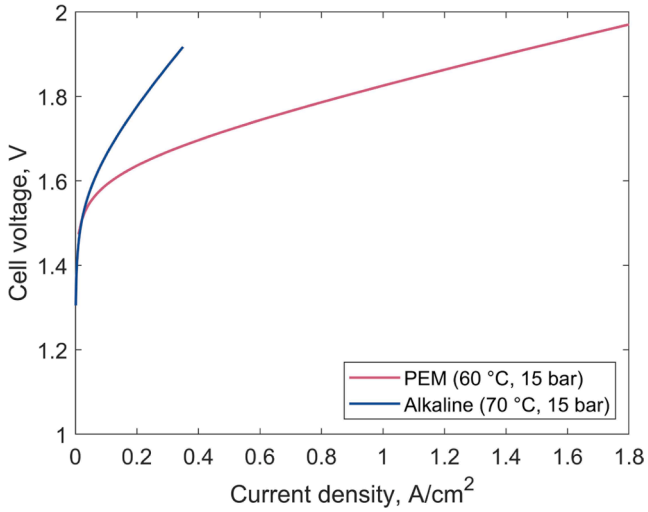


**Fig. 6.** Polarisation curves of the PEM and Alkaline electrolysers at the selected operating conditions: PEM at 15 bar and 60 °C and Alkaline at 15 bar and 70 °C.

The main technical input parameters are summarised in Table 8. A value of 15 bar was chosen for the electrolysis operating pressure to avoid a compression stage between the electrolyser and the methanation reactors. The operating temperature of the PEM electrolysis was set at 60 °C. A slightly higher value (70 °C) was instead considered for the alkaline technology [4,58]. The maximum operating current density for the PEM device was set at 1.8 A/$cm^2$. For the alkaline device, a maximum value of 0.35 A/$cm^2$ was used, in accordance with the assumptions of Parra *et al.* [59] and Buttler *et al.* [4]. For both technologies, the electricity demand due to the Balance of Plant (BoP) of the electrolyser was also considered for estimating the efficiency of the electrolyser system (stack + BoP). More specifically, the BoP includes the following subsystems: power supply, deionised water circulation, cooling circuit and hydrogen processing. The BoP demand was assumed to be 10% of the nominal power of the electrolyser system [60,61] and was set constant over the entire operating range, i.e., it is not dependent on the operating point [61].

A 1 MW-size module was considered for both PEM and alkaline systems. Electrolysers with larger capacities were supposed to be composed of more modules (of 1 MW each) in parallel [59].

For the sake of comparison, Fig. 6 shows the polarisation curves of the PEM and alkaline electrolysers at the selected working conditions. The PEM device can achieve a much higher current density, i.e., hydrogen production per unit of active area. This leads to a greater compactness of the PEM stack compared to the alkaline one. On the other hand, the capital cost of the PEM technology is currently higher than that of the alkaline technology [62]. Also, the lifetime of PEM stack is lower due to the higher degradation rate [51].

The nominal efficiency values derived from the model (LHV basis) are in line with data from the literature [4,63]. Under nominal conditions, an efficiency of 56.2% (59.28 kWh/kg) was determined for the alkaline system (stack + BoP), while a slightly higher value of about

**Table 8**
Main technical input parameters of ALK and PEM electrolysers [4,58–61].

| | Alkaline | PEM | Unit |
|---|---|---|---|
| **Operating temperature** | 70 | 60 | °C |
| **Operating pressure** | 15 | 15 | bar |
| **System minimum power** (% of nominal power) | 15 | 10 | % |
| **Max. current density** | 0.35 | 1.8 | A/$cm^2$ |
| **BoP electricity consumption** (% of nominal power) | 10 | 10 | % |

**Table 9**
Sizing results of the electrolysis section for an SNG production of 500 $m^3_{(NTP)}$/h.

| Components | ALK | PEM | Unit |
|---|---|---|---|
| Electrolyser (stack + BoP) | 10.6 | 10.4 | MW |
| Water storage tank | 32.1 | 32.1 | $m^3$ |
| Water pump | 1.4 | 1.4 | kW |
| Hydrogen compressor | 146.8 | 146.8 | kW |
| Air cooler | 29.7 | 29.7 | $m^2$ |
| Hydrogen storage tank | 442.4 | 442.4 | $m^3$ |

57.1% (58.39 kWh/kg) was computed for the PEM system (stack + BoP).

Since the power generated by the WI plant is usually higher than the nominal power of the electrolyser (to ensure that the share of electricity supplied to the electrolyser is renewable), the operating point of the electrolyser was set before the energy simulation of the PtG plant. Specifically, in accordance with other techno-economic assessments [59], the electrolyser was assumed to operate in nominal conditions.

A water feeding pump and a water storage tank are included into the system to reintegrate the water consumed by the electrolyser reaction and to ensure continuous operation in case of maintenance or failure of the water feeding line. The water pump was designed to increase the water pressure from ambient pressure to the operating pressure of the electrolyser. The isentropic and electromechanical efficiencies of the pump were assumed to be 0.8 and 0.9, respectively [23]. A specific water consumption of 15 L/kg of $H_2$ was considered for both PEM and alkaline systems [51]. The water storage tank was sized to provide a water supply for 12 h at nominal operating conditions of the electrolyser.

A pressurised hydrogen storage tank (maximum pressure of 90 bar) was also added to allow continuous supply of hydrogen to the methanation section during maintenance or failure of the electrolyser system or when the electricity generated by the WI is insufficient to meet the electrical load of the electrolyser system. The storage autonomy of the hydrogen storage tank was supposed equal to 12 h. The specific power consumption of the hydrogen compressor was calculated considering the isentropic and electromechanical efficiencies equal to 0.75 and 0.95, respectively [23].

Table 9 shows the main sizing results of the hydrogen production section. To cover the hydrogen demand for SNG production of 500 $m^3$/h, about 10.4–10.6 MW of electrolysis are needed. The sizes of the water and hydrogen storage are the same for the ALK and PEM systems since the same storage autonomy was assumed. The sizes of the other auxiliary components (i.e., water pump, hydrogen compressor and related air cooler) are also identical since, as previously reported, the same values for water consumption and operating pressure were supposed for both electrolysis typologies [64,65].

### 2.4. Methanation unit

As shown in Fig. 7, the methanation section consists of three refrigerated tube-bundle fixed-bed reactors, which were modelled as one-dimensional plug flow reactors [20,66], using an explicit first-order approach. Hydrogen is fed directly into the first reactor, whereas $CO_2$ is split into three streams (and sent to the three reactors) for thermal management of the Sabatier reaction. The gas streams entering the reactors are pre-heated by the products in head–tail heat exchangers to reach the reactor inlet temperature. The tube-bundle fixed-bed reactors are refrigerated by using boiling water, recovering the reaction heat and producing saturated steam. Water vapour is condensed between the second and the third reactor to increase the $CO_2$ conversion in the final reactor. The SNG recovered from the final condensation stage must be purified to remove unconverted hydrogen and reduce water moisture, so as to achieve natural gas grid specifications [34].

The design and the operating conditions of the reactors were calculated using a 1D pseudo-homogeneous reactor model, where the main assumptions of the calculation are perfect mixing and properties equal to inlet conditions of the discretisation step. The thermodynamic and transport properties of the pure components and of the gas mixture were estimated according to the equations reported by Todd and Young [67].

**Table 10**
Methanation unit characteristics and operating parameters for an SNG production of 500 $m^3_{(NTP)}$/h.

| Parameter | Value | Unit |
|---|---|---|
| $CO_2$ split fraction (Reactor I/II/III) | 35/46/19 | % |
| Tube diameter [20] | 0.05 | m |
| Tube/particle diameter ratio [20] | 10 | – |
| External porosity (cylindrical pellet, [68]) | 0.39 | – |
| Internal porosity [18] | 0.59 | – |
| Tortuosity [20] | 2.50 | – |
| Pure catalyst density [18] | 1274 | kg/$m^3$ |
| Equivalent catalyst thermal conductivity [18] | 0.67 | W/(m·K) |
| Catalyst heat capacity [18] | 1063 | J/(kg·K) |
| Maximum peak temperature [18,20] | 550 | °C |
| Input pressure | 15 | bar |
| Pressure drop | 0.6 | bar |

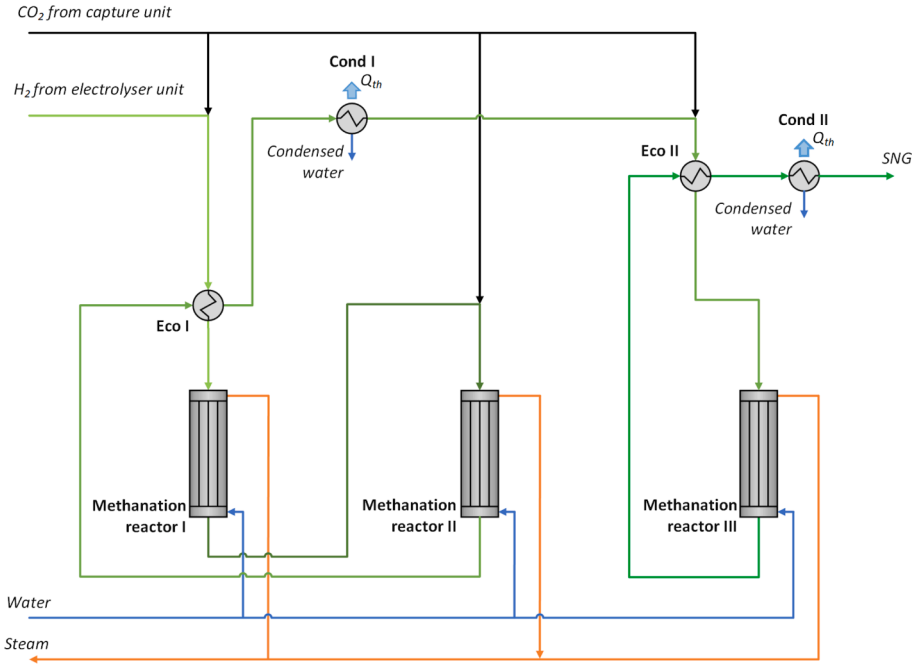


**Fig. 7.** Simplified process scheme of the methanation unit [20,24].

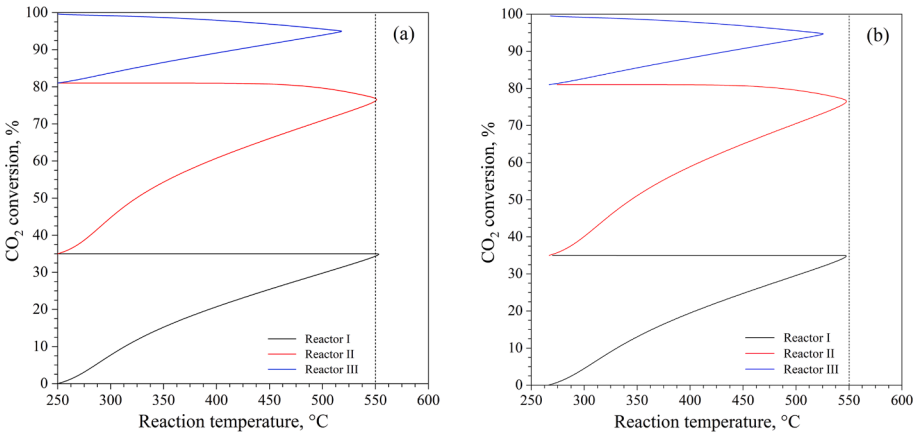


**Fig. 8.** $CO_2$ conversion vs. temperature within the 3 reactors by varying the operating load: (a) 60% and (b) 110% of the nominal productivity (500 $m^3_{(NTP)}$/h). For the sake of clarity, the design parameters are summarised in Table 10.

**Table 11**
Energy performance comparison for the considered carbon capture systems.

| Parameter | Absorption | | Adsorption | Unit |
|---|---|---|---|---|
| Sorbent type | Solvent A | Solvent B | $PEI/SiO_2$ | - |
| Flue gas flow rate | 7.8 | 7.8 | 10.3 | $km^3_{(NTP)}/h$ |
| Absorber/Adsorber $CO_2$ capture efficiency | 75 | 75 | 56.8 | % |
| Absorption/adsorption volume | 26.5 | 26.5 | 9.81* | $m^3$ |
| Desorption volume | 2.16 | 0.79 | 9.81* | $m^3$ |
| Regeneration temperature | 122 | 142 | 200 | °C |
| Specific electrical energy consumption | 227 | 163 | 549 | $kJ/kg_{(CO2)}$ |
| Net specific heat duty | 5.06 | 3.75 | 2.22 | $MJ/kg_{(CO2)}$ |
| Net specific cooling duty | −4.73 | −2.89 | −1.78 | $MJ/kg_{(CO2)}$ |

* Adsorption and desorption take place cyclically in the same reactors.

The reaction rate of $CO_2$ hydrogenation to methane was calculated according to the LHHW kinetic model of Koschany *et al.* [26], neglecting the RWGS reaction and the CO hydrogenation. This kinetic model was adopted in the present work due to the high activity and selectivity of the Ni/γ-$Al_2O_3$ catalyst even at relatively low temperatures. The radial dispersion and the overall heat transfer coefficient were predicted using the one-dimensional approach described by Schlereth and Hinrichsen [65]. Pressure drops were estimated by means of the Ergun equation.

To design the optimal configuration, a sensitivity analysis was conducted on the main operating parameters, and the main results are reported in the Supplementary Material. First, as shown in Figure S1, the effect of the $CO_2$ split fractions between the three reactors was investigated. The resulting $CO_2$ split fractions are 35%, 46% and 19% for the 1st, 2nd and 3rd reactor, respectively. These values are consistent with the results obtained by Giglio *et al.* [20]. Second, the effect of the operating load was considered in Figure S2. This is a crucial parameter for the thermal management of the reactors to avoid catalytic deactivation and hot spots within the reactors. Third, the number of tubes of the tube-bundle reactors was analysed in Figure S3 to determine the optimal cross-section area of the reactors. Fourth, the effect of the apparent catalytic bed density within the reactors is illustrated in Figure S4. And finally, the effect of the temperature of the cooling medium (boiling water) in the three reactors is summarised in Figure S5. This is an important parameter that could be used to control the methanation reaction within the reactors. Other design parameters were instead selected based on literature data; the catalyst properties and fixed design parameters are summarised in Table 10.

The catalytic pellets were partially diluted with inert pellets (e.g., $Al_2O_3$, SiC), reducing the apparent density of the catalytic bed to mitigate the intensity of the temperature peaks and the wide fluctuations linked to any small variation of the operating conditions. The number of tubes was designed to keep the maximum temperature below 550 °C. In order to control the temperature inside the reactors, the temperature of the cooling medium can range from 250 °C to 270 °C (i.e., the steam pressure varies from 38 bar to 47 bar) depending on the operating load (operating loads from 60% to 110% of nominal production were considered for the design). This temperature limit was set to avoid both rapid deactivation of the catalyst and structural issues related to the strength of the materials [18,20]. The gas hourly space velocity (GHSV) within the 1st, 2nd and 3rd reactor is 14200, 12310 and 3200 $m^3/(h{\cdot}m^3)$, respectively. The length of each reactor was selected to recover all the reaction heat and to achieve a $CO_2$ conversion of at least 99.5%. The tube-bundle heat exchangers and the condensation vessels were simulated using Aspen Plus. The temperature profiles by varying the operating load in the three reactors are shown in Fig. 8.

## 3. Key performance indicators

The energy and environmental performance of the PtG system was evaluated based on the key performance indicators described below.

- **Ratio of $CO_2$ Captured** (RCC, %): ratio between the amount of $CO_2$ captured and the total amount of $CO_2$ produced by the WI.

$$RCC = \frac{M_{CO_2,CC}}{M_{CO_2,WI}} \tag{11}$$

where $M_{CO_2,CC}$ (t/y) is the annual amount of $CO_2$ captured and $M_{CO_2,WI}$ (t/y) is the total amount of $CO_2$ produced by the WI. In our case this indicator also represents the reduction in $CO_2$ emissions, as all the electricity consumed by the PtG system comes from a renewable source.

- **Specific $CO_2$ avoided** ($m_{CO2}$, kg/MWh): reduction of $CO_2$ emissions to the atmosphere per MWh of SNG produced by the PtG system.

- **Specific water consumption** ($m_{H2O}$, kg/MWh): water consumed per MWh of SNG produced by the PtG system.
- **Global energy efficiency of the PtG system** ($\eta_{gl}$, %): it is evaluated as the ratio between the chemical energy of the produced SNG and the total consumption of electrical and thermal energy.

$$\eta_{gl} = \frac{V_{SNG} \cdot LHV_{SNG}}{E_{el} + Q_{th}} \quad (12)$$

where $V_{SNG}$ ($m^3$/y) is the annual SNG production, $LHV_{SNG}$ (MJ/$m^3$) is the SNG lower heating value, $E_{el}$ (MJ/y) is the annual electrical energy consumption of the PtG system and $Q_{th}$ (MJ/y) is the annual thermal energy consumption of the PtG system.

- **Specific Plant Energy Consumption for $CO_2$ Avoided** (SPECCA, MJ/kg): it is defined as the amount of electrical and thermal energy consumed to avoid the emission of one kg of $CO_2$ (in this KPI, power and heat are both computed in terms of MJ, even if the exergetic content of the heat is much lower compared to power).

$$SPECCA = \frac{E_{el} + Q_{th}}{M_{CO_2,CC} \cdot 1000} \quad (13)$$

## 4. Results and discussion

### 4.1. Carbon capture system comparison

Table 11 reports the performances of the different carbon capture techniques analysed in this work. The $CO_2$ adsorption system has the lowest specific heat duty: 2.22 MJ/$kg_{(CO2)}$ compared to 5.06 MJ/$kg_{(CO2)}$ and 3.75 MJ/$kg_{(CO2)}$ for the absorption systems with solvent A and B, respectively. On the other hand, the adsorption system is characterised by the lowest carbon capture efficiency (56.8%), resulting in a higher intercepted flue gas flow rate and higher specific electricity consumption for gas compression: 549 MJ/$kg_{(CO2)}$ versus 227 MJ/$kg_{(CO2)}$ (absorption with solvent A) and 163 MJ/$kg_{(CO2)}$ (absorption with solvent B). Another advantage of the technology with solid sorbents is the compactness of the system, due to the small volume of the adsorption reactor compared to the volume of the absorption and desorption columns.

### 4.2. Thermal integration

The hydrogenation of $CO_2$ to methane is a strongly exothermic reaction (-165 kJ/mol). According to the literature, the heat of reaction is usually recovered using boiling water and producing saturated steam in the range of 250 to 270 °C [8,20,22]. The saturated steam can then be fed into the carbon capture section and used to regenerate the liquid or solid sorbent [32,33]. After condensation, the hot water can be recirculated back to the methanation section. This thermal integration reduces the consumption of externally generated steam, with consequent reduction in the operating costs of the system.

#### 4.2.1. Methanation section energy balance

Concerning the methanation section, the reactors must be tightly thermally integrated to recover the sensible heat of the product gases, preheating the gases entering the reactors and condensing water vapor [20,23,24]. The temperature of the hot gas stream at the outlet of the economisers (Eco I and Eco II, see Fig. 7) was selected to avoid corrosion phenomena inside the heat exchanger. Corrosion occurs in the presence of a biphasic mixture, which could form if all the available heat is recovered to preheat the gas mixture.

Following the approach proposed by Giglio *et al.* [20], a pinch analysis was performed to design an optimal heat exchanger network (see Fig. 7). The stream exiting the second methanation reactor is used to preheat the stream entering the first reactor, by using an economiser (Eco I). The stream at the inlet of the third reactor is heated, in a head–tail heat exchanger, by using the stream exiting the same reactor (Eco II). The heat recovered in the two economisers is 169.0 kW (Eco I) and 78.6 kW (Eco II) for an SNG production of 500 $m^3_{(NTP)}$/h. Condensation of the water vapour and cooling of the gas streams require a total of 479.3 kW, which takes place in two coolers, one placed between the second and third reactor (Cond I, −389.1 kW) and the other at the outlet of the third reactor (Cond II, −90.1 kW).

#### 4.2.2. Integration between carbon capture and methanation units.

The methanation section of the PtG system is characterised by a large steam production of about 3.80 MJ/$kg_{(CO2)}$ (saturated steam at T ≥ 250 °C), coming from the cooling of the three reactors. This amount of heat can be easily recovered and used to meet a large part or even the entire heat demand of the carbon capture unit for sorbent regeneration [32,33]. As shown in Table 12, we estimate that the methanation section can cover about 75% of the heat duty of an absorption PCC unit using solvent A (5.06 MJ/$kg_{(CO2)}$); the remaining 25% (1.26 MJ/$kg_{(CO2)}$) needs to be supplied from the WI plant. For all the other configurations analysed, the steam production from the methanation section is sufficient to meet the total heat demand of the PCC unit, thus eliminating the need for steam from the WI.

### 4.3. Plant performance

The balances (energy and mass) and performance of the PtG configurations are summarised in Fig. 9, Fig. 10 and Table 13. As shown in Table 13, the PtG system produces about $3.9 \cdot 10^6$ $m^3_{(NTP)}$/y of SNG, with an electricity consumption of 81682 MWh/y to 83660 MWh/y, a thermal energy consumption of 0 MWh/y to 2538 MWh/y, and a cooling duty of −36842 MWh/y to −41627 MWh/y, depending on the system configuration considered. Regarding the cooling consumption, more than 70% is required for cooling the electrolyser (-28314 MWh/y for the ALK electrolyser and −27144 MWh/y for the PEM electrolyser), which is low-temperature heat and therefore difficult to recover.

The $CO_2$ required for the methanation process is supplied entirely by the carbon capture unit and accounts for about 3.8% of the total $CO_2$ emissions from the WI, which is lower than the biogenic $CO_2$ emissions. Therefore, the SNG produced by the PtG plant can be considered carbon–neutral and, by injecting it into the grid, it will substitute an equivalent amount of natural gas thus resulting in a net $CO_2$ emissions reduction equal to the $CO_2$ captured. This corresponds to a specific reduction in $CO_2$ emissions ($m_{CO2}$) of 190 kg/$MWh_{(SNG)}$ (Table 13). The

**Table 12**
Thermal integration of the methanation unit with the carbon capture unit.

| Parameter | System configurations | | | Unit |
|---|---|---|---|---|
| | Conf. 1<br>Conf. 4 | Conf. 2<br>Conf. 5 | Conf. 3<br>Conf. 6 | |
| Carbon capture technology | Absorption Solvent A | Absorption Solvent B | Adsorption $PEI/SiO_2$ | – |
| Heat available from methanation | −3.80 | −3.80 | −3.80 | MJ/$kg_{(CO2)}$ |
| Carbon capture heat duty | 5.06 | 3.75 | 2.22 | MJ/$kg_{(CO2)}$ |
| Thermal energy balance | 1.26 | −0.05 | −1.58 | MJ/$kg_{(CO2)}$ |

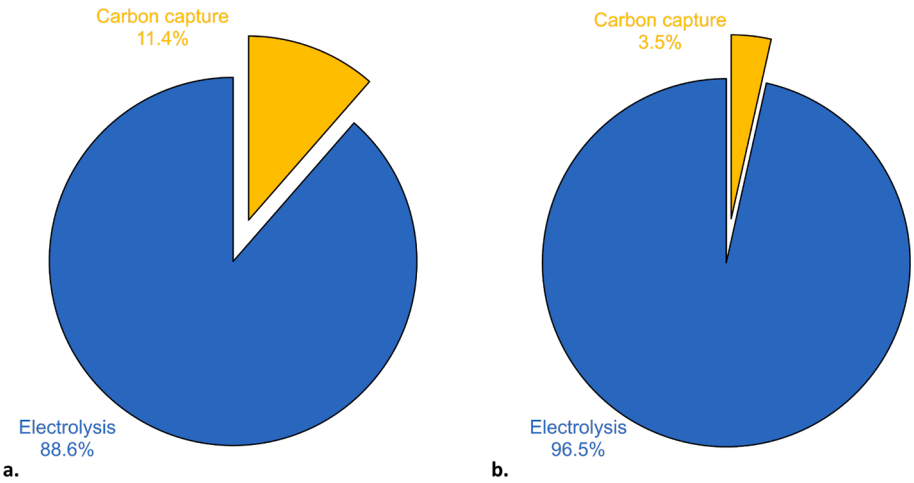


**Fig. 9.** Energy consumption share (electrical and thermal) of the PtG system in the reference configuration (Conf. 1) without (a.) and with (b.) thermal integration between the carbon capture and methanation units.

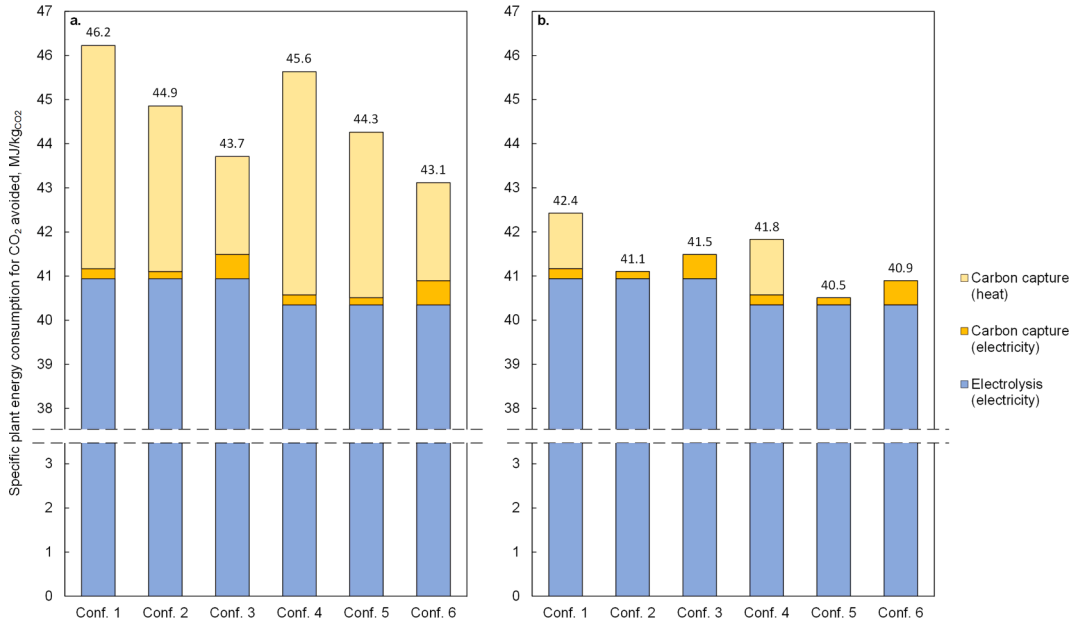


**Fig. 10.** Breakdown of the Specific Plant Energy consumption for $CO_2$ avoided (SPECCA) for the six configurations studied: (a) without and (b) with thermal integration between the carbon capture unit and the methanation unit.

specific water consumption ($m_{H2O}$), for hydrogen production and for the absorption unit makeup, ranges from 547 kg/$MWh_{(SNG)}$ to 627 kg/$MWh_{(SNG)}$, where the lowest value of 547 kg/$MWh_{(SNG)}$ was obtained for Conf. 3 and Conf. 6.

In all six system configurations, when considering thermal integration, more than 95% of the total energy consumption is consumed in the electrolysis section for hydrogen production, while less than 5% is consumed in the carbon capture unit. For example, as shown in Fig. 9b, in the reference configuration (Conf. 1), the electricity supplied to the electrolyser accounts for about 96.5% of the total energy consumption of the system (85547 MWh/y), while the carbon capture unit accounts for 3.5%. A slightly different breakdown is obtained if there is no heat recovery between the methanation unit and the carbon capture unit (see Fig. 9a). In this case, the heat required for sorbent regeneration in the carbon capture unit must be supplied entirely by the WI plant. The consumption of the carbon capture unit increases from 2538 MWh/y to 10200 MWh/y. This corresponds to 11.4% of the total energy consumption of the system, which increases to 93209 MWh/y.

As can be seen in Fig. 10a, when there is no thermal integration between the methanation section and the PCC section, the SPECCA indicator ranges from 43.1 MJ/$kg_{(CO2)}$ to 46.2 MJ/$kg_{(CO2)}$. Thermal integration leads to an improvement in the energy performances, as shown by the SPECCA values of Fig. 10b, which are in the range of 40.5 MJ/$kg_{(CO2)}$ to 42.4 MJ/$kg_{(CO2)}$ (around 5% decrease for Conf. 3 and Conf. 6 and 8% decrease for Conf. 1, 2, 4 and 5). Compared to the absorption PCC solutions, the adsorption PCC technology requires less thermal energy, which favors Conf. 3 and Conf. 6 over the other configurations if no thermal integration is performed. On the other hand, the adsorption technique requires more electricity because of the lower $CO_2$ capture efficiency, which increases the flue gas flow rate required to produce the target amount of $CO_2$. Therefore, when the PtG system is thermally integrated, the most promising solutions (with fixed electrolyser technology) are Conf. 2 and Conf. 5 since they have the lowest electrical consumption and their heat duty can be fully covered by thermal integration.

Focusing on the thermally-integrated solutions, the global energy

**Table 13**
Mass and energy balance of the PtG system in the different configuration proposed and resulting KPIs with thermal integration between carbon capture and methanation unit.

| Parameter | Symbol | Conf. 1 | Conf. 2 | Conf. 3 | Conf. 4 | Conf. 5 | Conf. 6 | Unit |
|---|---|---|---|---|---|---|---|---|
| Carbon capture technology | | Absorption | Absorption | TSA | Absorption | Absorption | TSA | |
| $CO_2$ sorbent | | MEA | MEA/[bpy][BF4] | PEI/$SiO_2$ | MEA | MEA/[bpy][BF4] | PEI/$SiO_2$ | |
| Electrolyser technology | | Alkaline | Alkaline | Alkaline | PEM | PEM | PEM | |
| Waste incinerator $CO_2$ emissions | $M_{CO2,\ WI}$ | 189.9 | 189.9 | 189.9 | 189.9 | 189.9 | 189.9 | kt/y |
| $CO_2$ captured | $M_{CO2,\ CC}$ | 7.26 | 7.26 | 7.26 | 7.26 | 7.26 | 7.26 | kt/y |
| $H_2$ to methanation | | 1.33 | 1.33 | 1.33 | 1.33 | 1.33 | 1.33 | kt/y |
| $O_2$ produced | | 10.64 | 10.64 | 10.64 | 10.64 | 10.64 | 10.64 | kt/y |
| SNG produced | $V_{SNG}$ | 3900 | 3900 | 3900 | 3900 | 3900 | 3900 | $km^3_{(NTP)}/y$ |
| **SNG produced** | $\mathbf{E_{SNG}}$ | 38155 | 38155 | 38155 | 38155 | 38155 | 38155 | MWh/y |
| **Electrical energy consumption** | $\mathbf{E_{el}}$ | **83009** | **82880** | **83660** | **81811** | **81682** | **82462** | **MWh/y** |
| Carbon capture unit | | 457 | 328 | 1108 | 457 | 328 | 1108 | MWh/y |
| Methanation unit | | 0 | 0 | 0 | 0 | 0 | 0 | MWh/y |
| Electrolyser unit | | 82552 | 82552 | 82552 | 81354 | 81354 | 81354 | MWh/y |
| **Thermal energy consumption** | $\mathbf{Q_{th}}$ | **2538** | **0** | **0** | **2538** | **0** | **0** | **MWh/y** |
| Carbon capture unit | | 10200 | 7567 | 4479 | 10200 | 7567 | 4479 | MWh/y |
| Heat recovery from methanation | | −7662 | −7567 | −4479 | −7662 | −7567 | −4479 | MWh/y |
| **Cooling consumption** | | **−41627** | **−38012** | **−38871** | **−40457** | **−36842** | **−37701** | **MWh/y** |
| Carbon capture unit | | −9537 | −5827 | −3598 | −9537 | −5827 | −3598 | MWh/y |
| Methanation unit | | −3776 | −3871 | −6959 | −3776 | −3871 | −6959 | MWh/y |
| Electrolyser unit | | −28314 | −28314 | −28314 | −27144 | −27144 | −27144 | MWh/y |
| **Water consumption** | | **23.92** | **23.11** | **20.88** | **23.92** | **23.11** | **20.88** | **kt/y** |
| Carbon capture unit | | 3.04 | 2.23 | 0 | 3.04 | 2.23 | 0 | kt/y |
| Electrolyser unit | | 20.88 | 20.88 | 20.88 | 20.88 | 20.88 | 20.88 | kt/y |
| **Equipment area** | | **1264** | **1261** | **1208** | **727** | **724** | **671** | **$m^2$** |
| Carbon capture unit | | 206 | 203 | 150 | 206 | 203 | 150 | $m^2$ |
| Electrolyser unit | | 1058 | 1,058 | 1,058 | 521 | 521 | 521 | $m^2$ |
| **Ratio of $CO_2$ captured** | **RCC** | **3.8%** | **3.8%** | **3.8%** | **3.8%** | **3.8%** | **3.8%** | **%** |
| **Specific $CO_2$ avoided** | $\mathbf{m_{CO2}}$ | **190** | **190** | **190** | **190** | **190** | **190** | **kg/MWh** |
| **Specific water consumption** | $\mathbf{m_{H2O}}$ | **627** | **606** | **547** | **627** | **606** | **547** | **kg/MWh** |
| **Global energy efficiency** | $\boldsymbol{\eta_{gl}}$ | **44.6** | **46.0** | **45.6** | **45.2** | **46.7** | **46.3** | **%** |
| **Specific Plant Energy Consumption for $CO_2$ avoided** | **SPECCA** | **42.4** | **41.1** | **41.5** | **41.8** | **40.5** | **40.9** | **MJ/kg** |

**Table 14**
Characteristics of the SNG produced and comparison with minimum Italian legislation requirement for grid injection.

| Parameter | Value | | | Italian legislation requirement [34] | Unit |
|---|---|---|---|---|---|
| Operating load | 60 | 100 | 110 | – | % |
| Volume flow rate | 300 | 500 | 550 | – | $m^3_{(NTP)}/h$ |
| Mass flow rate | 205.7 | 342.9 | 377.2 | – | kg/h |
| $CO_2$ molar fraction | 0.44 | 0.50 | 0.52 | < 3.0 | mol.% (dry basis) |
| $H_2$ molar fraction | 1.77 | 2.01 | 2.13 | < 0.5 | mol.% (dry basis) |
| $CH_4$ molar fraction | 97.79 | 97.49 | 97.35 | – | mol.% (dry basis) |
| $H_2O$ molar fraction | 0.321 | 0.321 | 0.321 | < 0.015 | vol.% |
| Pressure, bar | 14.6 | 14.4 | 14.4 | – | bar |
| Temperature | 14 | 14 | 14 | < 50 | °C |
| Wobbe index | 49.89 | 49.81 | 49.77 | 47.31 – 52.33 | $MJ/m^3_{(STP)}$ |

efficiency ($\eta_{gl}$) is in the range of 44.6% to 46.7%, while the SPECCA ranges from 40.5 $MJ/kg_{(CO2)}$ to 42.4 $MJ/kg_{(CO2)}$. Among all cases considered, Conf. 5 (PEM electrolyser and absorption PCC with solvent B) is the most efficient, with a $\eta_{gl}$ of 46.7% and a SPECCA of 40.5 $MJ/kg_{(CO2)}$. Conf. 1 (ALK electrolyser and absorption PCC with solvent A) presents, instead, the worst performance, with a $\eta_{gl}$ of 44.6% and a SPECCA of 42.4 $MJ/kg_{(CO2)}$. As shown in Fig. 10, the use of solvent B (instead of solvent A) in the absorption PCC unit leads to a reduction in the system energy consumption of around 1.3 $MJ/kg_{(CO2)}$, (SPECCA decreases from 42.4 $MJ/kg_{(CO2)}$ in Conf. 1 to 41.1 $MJ/kg_{(CO2)}$ in Conf. 2). The installation of a PEM electrolyser in place of an alkaline electrolyser further improves the SPECCA value by 0.6 $MJ/kg_{(CO2)}$ (SPECCA decreases from 41.1 $MJ/kg_{(CO2)}$ of Conf. 2 to 40.5 $MJ/kg_{(CO2)}$ of Conf. 5).

The different configurations proposed can also be compared considering the total area occupied by the equipment. In many industrial applications, such as WI plants, space might indeed be a limiting factor, making more compact system solutions preferable. In this regard, Conf. 6 is the most compact, with an estimated occupied area of about 671 $m^2$, while Conf. 1 is the least compact and requires an area of 1264 $m^2$. In particular, the hydrogen production section accounts for most of the space required, with 1058 $m^2$ for the ALK system (Conf. 1) and 521 $m^2$ for the PEM system (Conf. 6).

## 5. Technical considerations

### 5.1. Characteristics of the SNG

The characteristics of the SNG depend slightly on the operating load of the methanation unit. More specifically, the overall $CO_2$ conversion decreases from 99.6% to 99.5% when the operating load is increased from 60% to 110%. Table 14 shows that the $CO_2$ concentration in the produced SNG complies with the Italian legislation limit for biogas injection into the natural gas grid (i.e., less than 3.0 mol.%) [34]; however, the hydrogen content is higher than the prescribed limit of 0.5 mol.% [34]. This means that the SNG must be purified, for example, by means of membranes [25]. Furthermore, SNG contains ~ 0.032 mol.% of water; therefore, it must be dehydrated to reach the Italian legislation limit (dew point at −5 °C at 70 barg) [34], for example, by using zeolites or membranes [25]. Finally, the Wobbe index is included in the range of acceptance (i.e., 47.31 $MJ/m^3_{(STP)}$ to 52.33 $MJ/m^3_{(STP)}$).

### 5.2. Deterioration phenomena

The PtG plant could be damaged by corrosion phenomena that occur under common operating conditions. For this reason, all equipment must be selected to minimise wear, maintenance costs and investment costs.

Deterioration phenomena occur during absorption of $CO_2$ with MEA or MEA/IL aqueous solutions; more specifically, MEA, $CO_2$ and $O_2$ concentrations, along with temperature, are the main causes of corrosion [69]. According to Kittel *et al.* [69], the upper part of the $CO_2$ stripping column is the most affected by deterioration, reaching a corrosion rate of 1 mm/y for carbon steel. However, stainless steel showed good resistance, keeping the corrosion rate below 5 μm/y. Furthermore, there are two other degradation phenomena: (i) the formation of thermally stable salts due to oxidation when traces of $O_2$, $SO_x$, $NO_x$ and fly-ashes are present in the treated flue gas, and (ii) the thermal degradation of ammines during desorption [70,71]. Among all the degradation compounds, ammonia and acetaldehyde are the species with the highest concentrations, while N-nitrosamines must be strictly controlled due to their toxicity [72]. Moreover, the MEA degradation rate in a post-combustion carbon capture plant at industrial scale could range between 0.3 and 0.7 $kg_{(MEA)}/t_{(CO2)}$ [72], and the MEA concentration in the $CO_2$-lean flue gas is generally ~ 0.0004 vol% [72]. Regarding the MEA/IL aqueous blends, the ionic liquids generally show good resistance during $CO_2$ absorption/desorption under the operative conditions described in this work [73,74]. The decrease in the $CO_2$ removal efficiency could be mainly ascribed to the loss and degradation of MEA [38].

Concerning the $CO_2$ adsorption process, functionalised solid materials usually exhibit high $CO_2$ capacity, but they may be affected by degradation phenomena that reduce the performance of the adsorbent [75,76]. Non-functionalised solid sorbents generally show good thermal and mechanical stability under adsorption-regeneration conditions [73].

The $CO_2$-lean flue gas exiting the $CO_2$ capture unit could be sent to the chimney if it complies with all the emissions limits imposed by the legislation. More specifically, the Italian legislation (D.Lgs. 152/2006) sets these values: 10 $mg/Nm^3$ of powders, 10 $mg/Nm^3$ of total organic carbon, 50 $mg/Nm^3$ of $SO_2$, 200 $mg/Nm^3$ of $NO_2$, 30 $mg/Nm^3$ of $NH_3$ and 1 $mg/Nm^3$ of HF. If the $CO_2$-lean gas does not respect these restrictions, it must be treated to reduce the concentration of pollutants. The gas exiting the $CO_2$ capture unit could be fed at the inlet of the abatement system of the WI to treat the gas stream and remove pollutants. This solution can be pursued only if the abatement system is able to treat this excess flow rate; otherwise, a new gas treatment system must be installed.

Concerning low-temperature electrolysers, the lifetime of an alkaline electrolyser is between 60 kh and 90 kh and its degradation rate is lower than 3 μV/h (or 0.17 $\%_{LHV}$/kh). A PEM electrolyser generally has shorter lifetime (about 20 kh to 90 kh), and its degradation rate could reach 14 μV/h (or 0.78 $\%_{LHV}$/kh) [77,78]. The KOH aqueous solution used in alkaline electrolysers is extremely corrosive and stainless-steel alloys showed too low resistance; therefore, nickel–iron-chromium alloys are more suitable for this application [79].

As for the methanation process, the catalyst is affected by deactivation and needs to be replaced periodically. According to the literature, $Ni/Al_2O_3$ catalysts exhibit long-term deactivation mainly caused by the sintering of Ni particles [18,28,80]. Beierlein *et al.* [80] showed that the activity of the $Ni/Al_2O_3$ catalyst was 25% of the initial activity after 700 h of aging at 400 °C. They also developed a fast-aging procedure to

evaluate the performance of the aged $Ni/Al_2O_3$ catalyst, which can be used to estimate the optimal replacement rate of the catalyst [80]. Another crucial problem is given by the presence of $SO_2$ traces (from the flue gas of the WI) in the $CO_2$ stream produced by the PCC unit since Ni-based catalyst are extremely sensitive to sulphur poisoning. Wolf *et al.* [81] have demonstrated that 0.0005 vol% of $SO_2$ completely deactivated the catalyst in 24 h. Based on their correlations, we can estimate that annual replacement could be required if the $SO_2$ concentration in the gas supplied to the methanation unit is kept below $2{\cdot}10^{-6}$ vol%.

## 6. Conclusions

In this work, a PtG system for the production of SNG (500 $m^3_{(NTP)}/h$) and integrated in a WI plant was investigated. Part of the renewable energy (electricity and steam) produced by the WI is used for SNG production and all the $CO_2$ needed by the methanation is recovered from the flue gases of the WI, reducing its $CO_2$ emissions by about 3.8%.

A comprehensive evaluation of possible system configurations was performed, considering different electrolysis and carbon capture technologies. Specifically, hydrogen is produced using an alkaline or PEM electrolyser, while three different PCC technologies were analysed for $CO_2$ capture: (i) absorption using MEA solution liquid sorbent (Solvent A); (ii) absorption using MEA and IL solution liquid sorbent (Solvent B); and (iii) TSA using solid adsorbent ($PEI/SiO_2$). Mass and energy balances of the PtG plant were then assessed by modelling the main plant sections (carbon capture, electrolysis and methanation).

Results obtained from the process modelling show that a thermal integration between the methanation unit and the carbon capture unit greatly reduce the heat requirement of the system. In particular, the heat duty is reduced to zero when an absorption system with solvent B or a TSA system using $PEI/SiO_2$ adsorbent are considered for carbon capture. When thermal integration is performed, the total energy demand of the PtG plant is in the range of 81682 MWh/y to 85547 MWh/y, of which more than 95% is consumed by the electrolyser.

The performance of the PtG system was evaluated through the estimation of key performance indicators, such as the global plant efficiency ($\eta_{gl}$) and the Specific Plant Energy Consumption for $CO_2$ Avoided (SPECCA). The efficiency of the overall PtG plant (with thermal integration) was estimated in the range of 44.6% to 46.7% depending on the configuration. The maximum efficiency value of 46.7%, which corresponds to a SPECCA of 40.5 $MJ/kg_{(CO2)}$, was obtained for a PtG configuration using an absorption PCC system with solvent B and a PEM electrolyser (Conf. 5). The minimum value of 44.6% was instead computed for a system configuration using an absorption PCC system with solvent A and an alkaline electrolyser (Conf. 1), which is also characterised by the highest SPECCA value of 42.4 $MJ/kg_{(CO2)}$. When no thermal integration between the carbon capture unit and the methanation unit is considered, the SPECCA increases by about 5% to 9%, and the minimum value of 43.1 $MJ/kg_{(CO2)}$ is obtained for a system configuration using a TSA system and PEM electrolysis (Conf. 6).

Moreover, the composition of the produced SNG was compared with the requirements of the Italian legislation for grid injection: $CO_2$ concentration and Wobbe index are within the range of acceptance, but hydrogen and water content are above the maximum permissible limit. SNG must therefore undergo a final purification and dehydration process.

Future works will investigate the economic feasibility of the PtG system in order to assess the effectiveness of the different system configurations in terms of SNG production costs.

## CRediT authorship contribution statement

**Fabio Salomone:** Conceptualization, Formal analysis, Investigation, Methodology, Software, Validation, Visualization, Writing – original draft, Writing – review & editing. **Paolo Marocco:** Conceptualization, Formal analysis, Investigation, Methodology, Software, Validation, Visualization, Writing – original draft, Writing – review & editing. **Daniele Ferrario:** Formal analysis, Investigation, Methodology, Software, Validation, Visualization, Writing – original draft, Writing – review & editing. **Andrea Lanzini:** Supervision, Writing – review & editing. **Debora Fino:** Conceptualization, Funding acquisition, Project administration, Resources, Supervision. **Samir Bensaid:** Conceptualization, Funding acquisition, Project administration, Resources, Supervision, Writing – review & editing. **Massimo Santarelli:** Conceptualization, Funding acquisition, Project administration, Resources, Supervision, Writing – review & editing.

## Declaration of Competing Interest

The authors declare that they have no known competing financial interests or personal relationships that could have appeared to influence the work reported in this paper.

## Data availability

The data that has been used is confidential.

## Acknowledgements

The authors would like to acknowledge Iren S.p.A. for having supported and funded this research activity and Giulio Buffo for his great support and contribution to this work.

## Appendix A. Supplementary material

Supplementary data to this article can be found online at https://doi.org/10.1016/j.apenergy.2023.121200.

## References

[1] Intergovernmental Panel on Climate Change. Climate Change 2014: Synthesis Report. Geneva, Switzerland; 2014.
[2] Ince AC, Colpan CO, Hagen A, Serincan MF. Modeling and simulation of power-to-X systems: a review. Fuel 2021;304:121354. https://doi.org/10.1016/j.fuel.2021.121354.
[3] Van Leeuwen C, Mulder M. Power-to-gas in electricity markets dominated by renewables. Appl Energy 2018;232:258–72. https://doi.org/10.1016/j.apenergy.2018.09.217.
[4] Buttler A, Spliethoff H. Current status of water electrolysis for energy storage, grid balancing and sector coupling via power-to-gas and power-to-liquids: a review. Renew Sustain Energy Rev 2017;82:2440–54. https://doi.org/10.1016/j.rser.2017.09.003.
[5] Gorre J, Ruoss F, Karjunen H, Schaffert J, Tynjälä T. Cost benefits of optimizing hydrogen storage and methanation capacities for power-to-gas plants in dynamic operation. Appl Energy 2020;257. https://doi.org/10.1016/j.apenergy.2019.113967.
[6] Böhm H, Zauner A, Rosenfeld DC, Tichler R. Projecting cost development for future large-scale power-to-gas implementations by scaling effects. Appl Energy 2020;264. https://doi.org/10.1016/j.apenergy.2020.114780.
[7] Dutta S. A review on production, storage of hydrogen and its utilization as an energy resource. J Ind Eng Chem 2014;20(4):1148–56. https://doi.org/10.1016/j.jiec.2013.07.037.
[8] Götz M, Lefebvre J, Mörs F, Koch AM, Graf F, Bajohr S, et al. Renewable power-to-gas: a technological and economic review. Renew Energy 2016;85:1371–90. https://doi.org/10.1016/j.renene.2015.07.066.
[9] Buffo G, Marocco P, Ferrero D, Lanzini A, Santarelli M. Power-to-X and power-to-power routes. Solar Hydrogen Product: Processes Syst Technol 2019:530–75. https://doi.org/10.1016/b978-0-12-814853-2.00015-1.
[10] Rozzi E, Minuto FD, Lanzini A, Leone P. Green synthetic fuels: renewable routes for the conversion of non-fossil feedstocks into gaseous fuels and their end uses. Energies (Basel) 2020;13(2). https://doi.org/10.3390/en13020420.
[11] Science Advice for Policy by European Academies (SAPEA). Novel carbon capture and utilisation technologies, no. 2 https://doi.org/10.2777/01532.
[12] Boot-Handford ME, Abanades JC, Anthony EJ, Blunt MJ, Brandani S, Mac Dowell N, et al. Carbon capture and storage update. Energy Environ Sci 2014;7(1):130–89. https://doi.org/10.1039/c3ee42350f.
[13] MacDowell N, Florin N, Buchard A, Hallett J, Galindo A, Jackson G, et al. An overview of $CO_2$ capture technologies. Energy Environ Sci 2010;3(11):1645. https://doi.org/10.1039/c004106h.
[14] Chao C, Deng Y, Dewil R, Baeyens J, Fan X. Post-combustion carbon capture. Renew Sustain Energy Rev 2020;138:110490. https://doi.org/10.1016/j.rser.2020.110490.

[15] Notz R, Mangalapally HP, Hasse H. Post combustion $CO_2$ capture by reactive absorption: pilot plant description and results of systematic studies with MEA. Int J Greenhouse Gas Control 2012;6:84–112. https://doi.org/10.1016/j.ijggc.2011.11.004.

[16] Dijkstra JW, Walspurger S, Elzinga GD, Pieterse JAZ, Boon J, Haije WG. Evaluation of postcombustion $CO_2$ capture by a solid sorbent with process modeling using experimental $CO_2$ and $H_2O$ adsorption characteristics. Ind Eng Chem Res 2018;57(4):1245–61. https://doi.org/10.1021/acs.iecr.7b03552.

[17] Hägg MB, Lindbråthen A, He X, Nodeland SG, Cantero T. Pilot demonstration-reporting on $CO_2$ capture from a cement plant using hollow fiber process. Energy Procedia 2017;114(1876):6150–65. https://doi.org/10.1016/j.egypro.2017.03.1752.

[18] Morosanu EA, Salomone F, Pirone R, Bensaid S, Bensaid S. Insights on a methanation catalyst aging process: aging characterization and kinetic study. Catalysts 2020;10(3):283. https://doi.org/10.3390/catal10030283.

[19] Mazza A, Salomone F, Arrigo F, Bensaid S, Bompard E, Chicco G. Impact of Power-to-Gas on distribution systems with large renewable energy penetration. Energy Convers Manage: X 2020;7:100053. https://doi.org/10.1016/j.ecmx.2020.100053.

[20] Giglio E, Deorsola FA, Gruber M, Harth SR, Morosanu EA, Trimis D, et al. Power-to-gas through high temperature electrolysis and carbon dioxide methanation: reactor design and process modeling. Ind Eng Chem Res 2018;57(11):4007–18. https://doi.org/10.1021/acs.iecr.8b00477.

[21] Marocco P, Morosanu EA, Giglio E, Ferrero D, Mebrahtu C, Lanzini A, et al. $CO_2$ methanation over Ni/Al hydrotalcite-derived catalyst: experimental characterization and kinetic study. Fuel 2018;225:230–42. https://doi.org/10.1016/j.fuel.2018.03.137.

[22] Rönsch S, Schneider J, Matthischke S, Schlüter M, Götz M, Lefebvre J, et al. Review on methanation - from fundamentals to current projects. Fuel 2016;166:276–96. https://doi.org/10.1016/j.fuel.2015.10.111.

[23] Giglio E, Lanzini A, Santarelli M, Leone P. Synthetic natural gas via integrated high-temperature electrolysis and methanation: Part I—Energy performance. J Energy Storage 2015;1(1):22–37. https://doi.org/10.1016/j.est.2015.04.002.

[24] Salomone F, Giglio E, Ferrero D, Santarelli M, Pirone R, Bensaid S. Techno-economic modelling of a power-to-gas system based on SOEC electrolysis and $CO_2$ methanation in a RES-based electric grid. Chem Eng J 2019;377:120233. https://doi.org/10.1016/j.cej.2018.10.170.

[25] Morosanu EA, Saldivia A, Antonini M, Bensaid S. Process modeling of an innovative power to LNG demonstration plant. Energy Fuel 2018;32(8):8868–79. https://doi.org/10.1021/acs.energyfuels.8b01078.

[26] Koschany F, Schlereth D, Hinrichsen O. On the kinetics of the methanation of carbon dioxide on coprecipitated NiAl(O)x. Appl Catal B 2016;181:504–16. https://doi.org/10.1016/j.apcatb.2015.07.026.

[27] Champon I, Bengaouer A, Chaise A, Thomas S, Roger AC. Carbon dioxide methanation kinetic model on a commercial Ni/$Al_2O_3$ catalyst. J CO2 Util 2019;34:256–65. https://doi.org/10.1016/j.jcou.2019.05.030.

[28] Ewald S, Kolbeck M, Kratky T, Wolf M, Hinrichsen O. On the deactivation of Ni-Al catalysts in $CO_2$ methanation. Appl Catal A Gen 2019;570:376–86. https://doi.org/10.1016/j.apcata.2018.10.033.

[29] Giglio E, Lanzini A, Santarelli M, Leone P. Synthetic natural gas via integrated high-temperature electrolysis and methanation: Part II—Economic analysis. J Energy Storage 2015;2:64–79. https://doi.org/10.1016/j.est.2015.06.004.

[30] Haider J, Lee B, Choe C, Abdul Qyyum M, Shiung Lam S, Lim H. SNG production with net zero outflow of $CO_2$ in an integrated energy system: an energy and economic aspects. Energy Convers Manage 2022;270:116167. https://doi.org/10.1016/j.enconman.2022.116167.

[31] Gorre J, Ortloff F, Van Leeuwen C. Production costs for synthetic methane in 2030 and 2050 of an optimized power-to-gas plant with intermediate hydrogen storage. Appl Energy 2019;253:113594. https://doi.org/10.1016/j.apenergy.2019.113594.

[32] Chauvy R, Dubois L, Lybaert P, Thomas D, De Weireld G. Production of synthetic natural gas from industrial carbon dioxide. Appl Energy 2020;260:114249. https://doi.org/10.1016/j.apenergy.2019.114249.

[33] Chauvy R, Dubois L, Thomas D, De. Weireld G. Techno-economic feasibility and sustainability of an integrated carbon capture and conversion process to synthetic natural gas. SSRN Electron J 2021;47:101488. https://doi.org/10.2139/SSRN.3811432.

[34] SR GAS. Codice di rete; 2016.

[35] National Energy Technology Laboratory (NETL), Cost and Performance Baseline for Fossil Energy Plants - Volume 1: Bituminous Coal and Natural Gas to Electricity; 2010.

[36] Huang Y, Zhang X, Zhang X, Dong H, Zhang S. Thermodynamic modeling and assessment of ionic liquid-based $CO_2$ capture processes. Ind Eng Chem Res 2014;53(29):11805–17. https://doi.org/10.1021/ie501538e.

[37] Zacchello B, Oko E, Wang M, Fethi A. Process simulation and analysis of carbon capture with an aqueous mixture of ionic liquid and monoethanolamine solvent. Int J Coal Sci Technol 2017;4(1):25–32. https://doi.org/10.1007/s40789-016-0150-1.

[38] Yang J, Yu X, Yan J, Tu S. $CO_2$ capture using amine solution mixed with ionic. liquid 2014;53(7):2790–9. https://doi.org/10.1021/ie4040658.

[39] Akinola TE, Oko E, Wang M. Study of $CO_2$ removal in natural gas process using mixture of ionic liquid and MEA through process simulation. Fuel 2019;236:135–46. https://doi.org/10.1016/j.fuel.2018.08.152.

[40] Canepa R, Wang M, Biliyok C, Satta A. Thermodynamic analysis of combined cycle gas turbine power plant with post- combustion $CO_2$ capture and exhaust gas. Recirculation 2012;227(2):89–105. https://doi.org/10.1177/0954408912469165.

[41] Intergovernmental Panel on Climate Change, IPCC Special Report Carbon Dioxide Capture and Storage, New York; 2005. doi: 10.1002/9783527818488.ch15.

[42] Léonard G. Optimal design of a $CO_2$ capture unit with assessment of solvent degradation; 2013.

[43] Zareiekordshouli F, Lashanizadehgan A, Darvishi P. Study on the use of an imidazolium-based acetate ionic liquid for $CO_2$ capture from flue gas in absorber/stripper packed columns: experimental and modelling. Int J Greenhouse Gas Control 2018;70:178–92. https://doi.org/10.1016/j.ijggc.2018.02.002.

[44] Mofarahi M, Khojasteh Y, Khaledi H, Farahnak A. Design of $CO_2$ absorption plant for recovery of $CO_2$ from flue gases of gas. turbine 2008;33:1311–9. https://doi.org/10.1016/j.energy.2008.02.013.

[45] Ahn H, Luberti M, Liu Z, Brandani S. Process configuration studies of the amine capture process for coal-fired power plants. Int J Greenhouse Gas Control 2013;16:29–40. https://doi.org/10.1016/j.ijggc.2013.03.002.

[46] Nelson TO, Coleman LJI, Mobley P, Kataria A, Tanthana J, Lesemann M, et al. Solid sorbent $CO_2$ capture technology evaluation and demonstration at Norcem's cement plant in Brevik, Norway. Energy Procedia 2014;63:6504–16. https://doi.org/10.1016/j.egypro.2014.11.686.

[47] Ntiamoah A, Ling J, Xiao P, Webley PA, Zhai Y. $CO_2$ Capture by temperature swing adsorption: use of Hot $CO_2$-rich gas for regeneration. Ind Eng Chem Res 2016;55(3):703–13. https://doi.org/10.1021/acs.iecr.5b01384.

[48] Cloete S, Giuffrida A, Romano MC, Zaabout A. The swing adsorption reactor cluster for post-combustion $CO_2$ capture from cement plants. J Clean Prod 2019;223:692–703. https://doi.org/10.1016/j.jclepro.2019.03.109.

[49] Aaron D, Tsouris C. Separation of $CO_2$ from flue gas: a review. Sep Sci Technol 2005;40:321–48. https://doi.org/10.1081/SS-200042244.

[50] Schmidt O, Gambhir A, Staffell I, Hawkes A, Nelson J, Few S. Future cost and performance of water electrolysis: an expert elicitation study. Int J Hydrogen Energy 2017;42(52):30470–92. https://doi.org/10.1016/j.ijhydene.2017.10.045.

[51] TRACTEBEL ENGINEERING S.A. and Hinicio. Study on early business cases for $H_2$ in energy storage and more broadly power-to-$H_2$ applications; 2017. p. 228.

[52] Marocco P, Ferrero D, Lanzini A, Santarelli M. Optimal design of stand-alone solutions based on RES + hydrogen storage feeding off-grid communities. Energy Convers Manage 2021;238:114147. https://doi.org/10.1016/j.enconman.2021.114147.

[53] Henao C, Agbossou K, Hammoudi M, Dubé Y, Cardenas A. Simulation tool based on a physics model and an electrical analogy for an alkaline electrolyser. J Power Sources 2014;250:58–67. https://doi.org/10.1016/j.jpowsour.2013.10.086.

[54] Han B, Steen SM, Mo J, Zhang FY. Electrochemical performance modeling of a proton exchange membrane electrolyzer cell for hydrogen energy. Int J Hydrogen Energy 2015;40(22):7006–16. https://doi.org/10.1016/j.ijhydene.2015.03.164.

[55] Ulleberg Ø. Modeling of advanced alkaline electrolyzers:a system simulation approach. Int J Hydrogen Energy 2003;28:21–33. https://doi.org/10.1016/S0360-3199(02)00033-2.

[56] Rahim AHA, Tijani AS. Modeling and analysis the effects of temperature and pressure on the gas-crossover in polymer electrolyte membrane electrolyzer. Int J Electr Comput Energet Electron Commun Eng 2015;10(1):1–7.

[57] Tsotridis G, Pilenga A. EU harmonized terminology for low-temperature water electrolysis for energy-storage applications; 2018.

[58] Marocco P, Ferrero D, Gandiglio M, Ortiz MM, Sundseth K, Lanzini A, et al. A study of the techno-economic feasibility of $H_2$-based energy storage systems in remote areas. Energy Convers Manage 2020;211:112768. https://doi.org/10.1016/j.enconman.2020.112768.

[59] Parra D, Patel MK. Techno-economic implications of the electrolyser technology and size for power-to-gas systems. Int J Hydrogen Energy 2016;41(6):3748–61. https://doi.org/10.1016/j.ijhydene.2015.12.160.

[60] Mayyas A, Ruth M, Pivovar B, Bender G, Wipke K. Manufacturing cost analysis for proton exchange membrane water electrolyzers; 2019.

[61] Godula-Jopek A, Stolten D. Hydrogen production by electrolysis. Wiley-VCH; 2015.

[62] Proost J. State-of-the art CAPEX data for water electrolysers, and their impact on renewable hydrogen price settings. Int J Hydrogen Energy 2019;44(9):4406–13. https://doi.org/10.1016/j.ijhydene.2018.07.164.

[63] Marocco P, Gandiglio M, Audisio D, Santarelli M. Assessment of the role of hydrogen to produce high-temperature heat in the steel industry. J Clean Prod 2023;388:135969. https://doi.org/10.1016/j.clepro.2023.135969.

[64] Pino FJ, Valverde L, Rosa F. Influence of wind turbine power curve and electrolyzer operating temperature on hydrogen production in wind–hydrogen systems. J Power Sources 2011;196(9):4418–26. https://doi.org/10.1016/j.jpowsour.2010.10.060.

[65] Schlereth D, Hinrichsen O. A fixed-bed reactor modeling study on the methanation of $CO_2$. Chem Eng Res Des 2014;92(4):702–12. https://doi.org/10.1016/j.cherd.2013.11.014.

[66] Giglio E, Pirone R, Bensaid S. Dynamic modelling of methanation reactors during start-up and regulation in intermittent power-to-gas applications. Renew Energy 2021;170:1040–51. https://doi.org/10.1016/j.renene.2021.01.153.

[67] Todd B, Young JB. Thermodynamic and transport properties of gases for use in solid oxide fuel cell modelling. J Power Sources 2002;110(1):186–200. https://doi.org/10.1016/S0378-7753(02)00277-X.

[68] Benyahia F, O'Neill KE. Enhanced voidage correlations for packed beds of various particle shapes and sizes. Part Sci Technol 2005;23(2):169–77. https://doi.org/10.1080/02726350590922242.

[69] Kittel J, Idem R, Gelowitz D, Tontiwachwuthikul P, Parrain G, Bonneau A. Corrosion in MEA units for $CO_2$ capture: Pilot plant studies. Energy Procedia 2009;1(1):791–7. https://doi.org/10.1016/j.egypro.2009.01.105.

[70] Gouedard C, Picq D, Launay F, Carrette PL. Amine degradation in $CO_2$ capture. I. A review. Int J Greenhouse Gas Control 2012;10:244–70. https://doi.org/10.1016/j.ijggc.2012.06.015.
[71] Fytianos G, Ucar S, Grimstvedt A, Hyldbakk A, Svendsen HF, Knuutila HK. Corrosion and degradation in MEA based post-combustion $CO_2$ capture. Int J Greenhouse Gas Control 2016;46:48–56. https://doi.org/10.1016/j.ijggc.2015.12.028.
[72] Azzi M, White S. Emissions from amine-based post-combustion $CO_2$ capture plants. Elsevier Ltd 2016. https://doi.org/10.1016/B978-0-08-100514-9.00020-2.
[73] Yu CH, Huang CH, Tan CS. A review of $CO_2$ capture by absorption and adsorption. Aerosol Air Qual Res 2012;12(5):745–69. https://doi.org/10.4209/aaqr.2012.05.0132.
[74] Kosmulski M, Gustafsson J, Rosenholm JB. Thermal stability of low temperature ionic liquids revisited. Thermochim Acta 2004;412(1–2):47–53. https://doi.org/10.1016/j.tca.2003.08.022.
[75] Srikanth CS, Chuang SSCC. Spectroscopic investigation into oxidative degradation of silica-supported amine sorbents for $CO_2$. Capture 2012;5(8):1435–42. https://doi.org/10.1002/cssc.201100662.
[76] Wang J, Huang L, Yang R, Zhang Z, Wu J, Gao Y, et al. Recent advances in solid sorbents for $CO_2$ capture and new development trends. Energy Environ Sci 2014;7(11):3478–518. https://doi.org/10.1039/C4EE01647E.
[77] Li Z, Zhang H, Xu H, Xuan J. Advancing the multiscale understanding on solid oxide electrolysis cells via modelling approaches: a review. Renew Sustain Energy Rev 2021;141:110863. https://doi.org/10.1016/j.rser.2021.110863.
[78] Carmo M, Fritz DL, Mergel J, Stolten D. A comprehensive review on PEM water electrolysis. Int J Hydrogen Energy 2013;38(12):4901–34. https://doi.org/10.1016/j.ijhydene.2013.01.151.
[79] Gras JM, Spiteri P. Corrosion of stainless steels and nickel-based alloys for alkaline water electrolysis. Int J Hydrogen Energy 1993;18(7):561–6. https://doi.org/10.1016/0360-3199(93)90175-A.
[80] Beierlein D, Häussermann D, Traa Y, Klemm E. Rapid aging as a key to understand deactivation of $Ni/Al_2O_3$ catalysts applied for the $CO_2$ methanation. Cat Lett 2022;152(10):2908–19. https://doi.org/10.1007/s10562-021-03884-2.
[81] Wolf M, Schüler C, Hinrichsen O. Sulfur poisoning of co-precipitated Ni–Al catalysts for the methanation of $CO_2$. J CO2 Util 2019;32:80–91. https://doi.org/10.1016/j.jcou.2019.03.003.